High resolution 3D P wave velocity structure beneath Tenerife Island (Canary Islands, Spain) based on tomographic inversion of active-source data

Araceli García-Yeguas,[1,2] Ivan Koulakov,[3] Jesús M. Ibáñez,[1,2] and A. Rietbrock[4]

Received 3 November 2011; revised 1 August 2012; accepted 2 August 2012; published 22 September 2012.

[1] We present a high resolution 3 dimensional (3D) P wave velocity model for Tenerife Island, Canaries, covering the top of Teide volcano (3,718 m a.s.l.) down to around 8 km below sea level (b.s.l). The tomographic inversion is based on a large data set of travel times obtained from a 3D active seismic experiment using offshore shots (air guns) recorded at more than 100 onshore seismic stations. The obtained seismic velocity structure is strongly heterogeneous with significant (up to 40%) lateral variations. The main volcanic structure of the Las Cañadas-Teide-Pico Viejo Complex (CTPVC) is characterized by a high P wave velocity body, similar to many other stratovolcanoes. The presence of different high P wave velocity regions inside the CTPVC may be related to the geological and volcanological evolution of the system. The presence of high P wave velocities at the center of the island is interpreted as evidence for a single central volcanic source for the formation of Tenerife. Furthermore, reduced P wave velocities are found in a small confined region in CTPVC and are more likely related to hydrothermal alteration, as indicated by the existence of fumaroles, than to the presence of a magma chamber beneath the system. In the external regions, surrounding CTPVC a few lower P wave velocity regions can be interpreted as fractured zones, hydrothermal alterations, porous materials and thick volcaniclastic deposits.

Citation: García-Yeguas, A., I. Koulakov, J. M. Ibáñez, and A. Rietbrock (2012), High resolution 3D P wave velocity structure beneath Tenerife Island (Canary Islands, Spain) based on tomographic inversion of active-source data, *J. Geophys. Res.*, *117*, B09309, doi:10.1029/2011JB008970.

1. Introduction

[2] Volcanic environments are typically complex regions of heterogeneous rock types, fluids and gases, and the associated volcanic hazard often has societal implications. Significant advances have been made in interpreting the early warning signs of volcanic eruptions based on the analysis of multiple geophysical and geochemical data, including seismicity, gas emissions and ground deformation; however, the interpretation of these data has to be based on a sound knowledge of the internal structure of the volcano edifice. Seismic tomography is a powerful tool providing reliable measurements of the structure of the Earth. Its application to volcanic environments has provided high-resolution images of several volcanoes and their surrounding regions (e.g., Etna [*Cardaci et al.*, 1993; *Aloisi et al.*, 2002], Redoubt [*Benz et al.*, 1996], Kilauea [*Dawson et al.*, 1999], Azores [*Zandomeneghi et al.*, 2008], or the Kluchevskoy volcano [*Koulakov et al.*, 2011], among others).

[3] Most of these studies are based on passive-source seismic recordings utilizing the arrival times of P and S waves from local earthquakes; however, the uneven distribution of earthquake hypocenters and their unknown locations significantly limit the resolution of the computed models. High quality imagery in passive seismic studies is based on joint inversion for source parameters and the velocity model and requires large number of evenly distributed stations operating for long time periods (several months to years). In practice, very few networks satisfying these requirements are available in volcanic regions given the complex topography, hazardous environment and difficulties with instrument installation and maintenance.

[4] Some of these problems can be solved by conducting a seismic active-source experiment based on artificial seismic signals recorded by a dense seismic station network operating for a relatively short period of time. Furthermore, higher frequencies in comparison to passive sources are excited increasing the resolution of the tomographic images. Onshore, the active sources are usually produced by chemical blasts

[1]Departamento de Física Teórica y del Cosmos, Facultad de Ciencias, University of Granada, Granada, Spain.
[2]Instituto Andaluz de Geofísica, University of Granada, Granada, Spain.
[3]Institute of Petroleum Geology and Geophysics, Novosibirsk, Russia.
[4]School of Environmental Sciences, University of Liverpool, Liverpool, UK.

Corresponding author: A. García-Yeguas, Departamento de Física Teórica y del Cosmos, Facultad de Ciencias, University of Granada, Granada ES-18071, Spain. (araceli@ugr.es)

0148-0227/12/2011JB008970

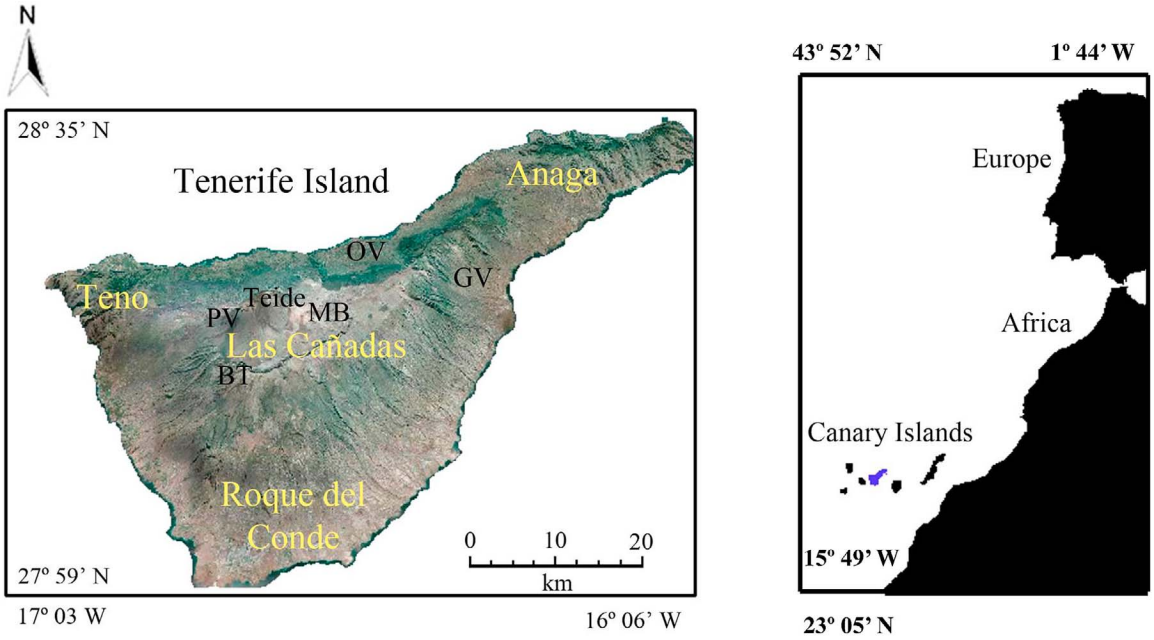

Figure 1. (left) Location of the main geological units at the Tenerife Island. Satellite image is shown for the onshore part. Indications: GV: Güimar Valley; OV: Orotova Valley; MB: Montaña Blanca; PV: Pico Viejo; BT: Boca Tauce volcano. (right) Location of the Tenerife Island (marked with blue) in respect to Europe and Africa.

(e.g., as Asama volcano [*Aoki et al.*, 2009]); however the use of such sources is strictly limited in most volcanic areas. When volcanic regions are close to the sea, air gun shots are a realistic alternative for generating signals. This scheme is widely used in experiments in volcanic areas, such as: Vesuvius [*Zollo et al.*, 2002], Campi Flegrei [*Zollo et al.*, 2003], Asama [*Aoki et al.*, 2009], Deception Island [*Zandomeneghi et al.*, 2009], Ascention Island [*Evangelidis et al.*, 2004], Izu-Bonin [*Calvert et al.*, 2008] and Montserrat Island [*Paulatto et al.*, 2010, 2012; *Shalev et al.*, 2010].

[5] This study focuses on the volcanic island of Tenerife (Canary Islands, Spain), an environment of high volcanic risk due to its eruptive history, morphology and population distribution. Tenerife Island has a high geomorphological complexity including the caldera system of CTPVC with the large Teide stratovolcano at its center, a large number of smaller volcanic cones, steep valleys and vertical cliffs. On the other hand, there are some preferred directions of alignment of volcanic systems. This wide variety of geomorphological and volcanological contrasts presents an important set of issues that are still debated. The last eruption occurred in 1909 (Chinyero volcano), after which volcanic activity was absent except for gas and fumarolic activity [*Pérez et al.*, 1996; *Hernández et al.*, 2000, 2004]. Recent seismic activity has been located offshore, as documented in the catalog of the Instituto Geográfico Nacional (IGN, Spain) for the last 20 years, with the exception of a few low magnitude events on land [*Almendros et al.*, 2000]. An unusual increase in seismic activity was observed on Tenerife between April and September 2004 —more than 500 earthquakes were recorded during this period, including some of moment magnitude (Mw) greater than 3.0, which were felt by the population of the island [*Almendros et al.*, 2007]. Activity decreased in the first half of 2005 to a normal level of about 10–20 events per month. On the basis of this unusual activity, a reawakening of the volcano was suggested [*García et al.*, 2006], though an eruption has not occurred yet.

[6] In January 2007, an active seismic experiment called TOM-TEIDEVS [*Ibáñez et al.*, 2008] was performed on Tenerife in order to obtain a P wave velocity tomographic image of this volcanic island. The present work describes the high resolution P wave velocity structure of Tenerife Island based on data obtained from this experiment. We show the velocity structure of the island from the top of Teide (3,718 m above sea level (a.s.l.).) to around 10,000 m below sea level (b.s.l.), covering a surface area of over 2,000 km2.

[7] The main objective of this paper is to help understand the structure and dynamics of this complex volcanic system and shed some new light on some of the open issues about its formation mechanism and evolution. In particular we address the hypothesis of a three-rift system underlying the island and determining its morphology [*Carracedo et al.*, 2009], the origin and evolution of the Las Canadas caldera and the existence of an active shallow magma chamber beneath Teide volcano.

2. Geological Setting

[8] Tenerife Island is a volcanic island of the Canary Islands archipelago (Spain) (Figure 1). The origin of the Canary Islands is a matter still under discussion; and although for a long time many authors postulated their relationship with a hot spot [e.g., *Canas et al.*, 1998], others insist on an unclear origin [i.e., *Anguita*, 2000]. Tenerife Island is situated in the Atlantic Ocean, off the NW coast of Africa, at latitude 28–29°N and longitude 16–17°W. With an area of 2,040 km3, it is the largest of the Canary Islands. Its topography is very heterogeneous, with basaltic and felsic lava flows, domes,

monogenetic cones, stratovolcanoes, calderas (Las Cañadas), and pyroclastic deposits, implying diverse volcanic processes. The most important complex is the CTPVC edifice, in the center of the island, formed by a caldera and a stratovolcano complex known as Pico Viejo-Teide in the middle. This caldera is elliptical, measuring 16 × 9 km, and it lies at 2000 m a.s.l.

[9] Two kinds of volcanism, fissure basaltic and explosive, took part in the formation of Tenerife Island. In the case of effusive volcanism, the eruptions are basaltic and the magma ascended through the mantle to the surface. The fissure basaltic volcanism is mainly located at the NE and NW ridges, and spreads over the southern part of the island. These eruptions produced 297 monogenetic cones on the island [*Dóniz et al.*, 2008; *Dóniz Páez*, 2009] and are the most common type of eruption. The recurrence period of this kind of eruption is short, meaning that an event in the near future is possible. Explosive eruptions involving phonolitic magma chambers [*Andújar et al.*, 2008] have given rise to the different phases of formation of the CTPVC. The last subplinian eruption, at Montaña Blanca (east flank of Teide), happened 2000 years ago [*Ablay et al.*, 1995].

[10] The documented volcanic history of the Canary Islands covers the last 500 years [*Romero*, 1991, 1992]. The first historical eruption took place at the NW-SE ridge (Figure 1), called Boca Cangrejo, in 1492. Sietefuentes volcanoes erupted in 1704; and Fasnia and Arafo volcanoes, located at the NE-SW ridge, erupted in 1705. The following year, 1706, saw the eruption of Garachico on the NW-SE ridge. The CTPVC underwent a basaltic eruption in 1798 involving the Chahorra Volcanoes. The most recent eruption recorded was in 1909, at El Chinyero volcano, by the NW-SE ridge.

[11] In the evolutionary context of Tenerife Island, as pointed out by *Schmincke* [2004], very little is known about the seamount stage of growth, although about 90% of the total volume of Tenerife corresponds to its submerged portion.

[12] Three main regions were formed in the initial stage (Figure 1): Roque del Conde (11.9–3.9 Ma), Teno massif (6.3–5.3 Ma) and Anaga massif (4.9–3.9 Ma) [e.g., *Thirlwall et al.*, 2000; *Huertas et al.*, 2002; *Pous et al.*, 2002; *Guillou et al.*, 2004; *Leonhardt and Soffel*, 2006; *Coppo et al.*, 2008; *Gottsmann et al.*, 2008].

[13] The CTPVC is the main volcanic edifice of the island at present. Different periods of activity can be identified in its evolution, separated by quiet gaps that are longer than the periods of activity [*Araña et al.*, 1994]. The sequence of events generating each constructive and destructive phase can be described as: 1. Continuous ascent of basaltic magma from the mantle; 2. formation of shallow phonolitic magma chambers, and thus, phonolitic eruptions with generation of basaltic eruptions in the center of the island; 3. formation of the caldera, with the partial or total destruction of the magma chamber; 4. eruption of basaltic magmas in the center of the island; 5. construction of a new phonolitic magmatic chamber in a different place, implying migration of the magma chamber to another sector of the central area.

[14] Two contrasting theories have been put forward to explain the origin of the Las Cañadas caldera. Some workers propose a vertical collapse mechanism [*Martí et al.*, 1997; *Martí and Gudmundsson*, 2000; *Coppo et al.*, 2008; *Gottsmann et al.*, 2008; *Martí et al.*, 2010], while others favor a side collapse followed by a giant landslide [*Navarro and Coello*, 1989; *Ancochea et al.*, 1998, 1999; *Cantagrel et al.*, 1999]. See *Blanco-Montenegro et al.*, 2011, for a review.

[15] Few studies explore the two or three rift axes surrounding the CTPVC, and their origin and evolution are likewise under discussion. *Carracedo* [1994] reports the existence of a convergent three-armed rift in Tenerife, with axes following NW-SE, NE-SW and N-S directions. He proposes that this rift system controlled the occurrence of volcanic activity from the basaltic shield stage to the present time. Carracedo based his interpretation on eruptive vent concentration and dike density observed in tunnels excavated while searching for water. However, alternative theories [*Martí et al.*, 1996; *Geyer and Martí*, 2010] suggest that regional tectonics have controlled the distribution of volcanism. In the southern half of Tenerife recent eruptive vents appear too scattered to represent an alignment [*Ancochea et al.*, 1995; *Hürlimann et al.*, 2004].

[16] What is known about the volcanic system at depth on Tenerife Island? Attempts to determine the internal structure of Tenerife Island using geophysical techniques have included resistivity measurements [*Pous et al.*, 2002; *Coppo et al.*, 2008]; aeromagnetic surveying [*Blanco-Montenegro et al.*, 2011], gravity [*Araña et al.*, 2000; *Gottsmann et al.*, 2008] and seismological studies [*Canales et al.*, 2000]. *Gottsmann et al.* [2008], showed, based on gravity data, that the core of the island is denser than its surroundings. *Canales et al.* [2000] observed higher P wave velocity in CTPVC wall beneath the Boca Tauce volcano (Figure 1), from inversion of active-source seismic data. This body, interpreted as a plutonic intrusion [*Canales et al.*, 2000], could play an important role in the evolution of the CTPVC, preventing the occurrence of landslides in the Southern and Western parts of the island. Recently, *Blanco-Montenegro et al.* [2011] presented 3D magnetic models of Tenerife from a high-resolution aeromagnetic survey. Their model supports the vertical collapse hypothesis for the origin of the Las Cañadas caldera. They also observed a high-magnetization region beneath the North flank of Teide-Pico Viejo, suggestive of a dense dike complex.

[17] The seismic activity of Tenerife Island is very limited. The catalog of the National Seismic Network (IGN, http://www.ign.es/ign/main/index.do) and other studies [*Del Pezzo et al.*, 1997; *Almendros et al.*, 2000, 2007] indicate that, with the exception the 2004–2005 seismic crises, there is a low occurrence of volcano-tectonic earthquakes and an absence of other volcanic signals such as long period events (LP) or tremors. Hence, the only way to obtain high-resolution seismic tomographic images is by using artificial sources, as in the TOM-TEIDEVS experiment.

3. Data and Method

3.1. Seismic Experiment

[18] The active seismic experiment TOM-TEIDEVS was carried out in January 2007 [*Ibáñez et al.*, 2008]. The project was led by the University of Granada and involved research groups from Spain, the UK, Italy, Ireland and Mexico (the TOM-TEIDEVS research group).

[19] The experiment consisted of the deployment of a dense seismic network on Tenerife Island and the shooting of air guns around the island. The Spanish oceanographic vessel R/V Hespérides fired shots using a 12 m long array consisting of six BOLT 1500LL with a total volume of 3520 cu.in.

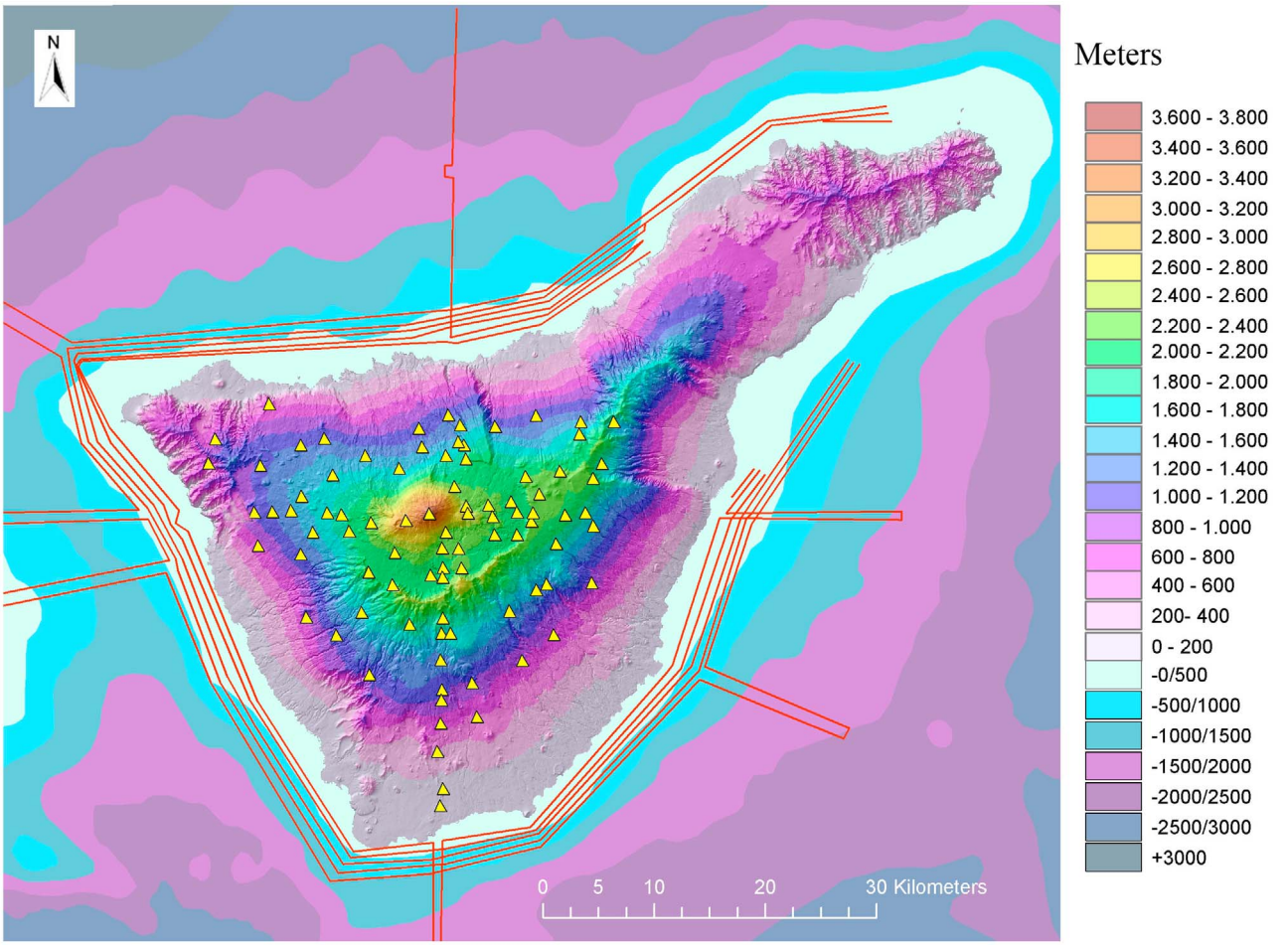

Figure 2. Experiment configuration. Red and orange dots represent shots fired in legs 1 and 2, respectively. Triangles show the seismic stations on Tenerife Island. Axes are in kilometers. Background is smoothed topography/bathymetry map.

(57.68 L). The air guns were shot every two minutes (6459 shots were fired in total), which corresponds to a shot separation of around 300 m (Figure 2). A total of 125 seismometers provided by various institutions from the UK, Italy and Spain were deployed on Tenerife Island. The majority of instruments were 100 Guralp CMG-6TD provided by the University of Liverpool, UK, with a bandwidth of 30 s to 100 Hz and continuously sampled at 200 Hz. The shooting program was divided into two separate legs. To improve ray coverage for the tomographic study some of the stations were relocated after the first leg. The full recording geometry is given in Figure 2. Altogether, 137 sites were occupied used to record the shots. The station distribution was chosen in view of the following criteria: (1) high-density station coverage in the area around CTPVC; (2) at least two straight reflection/refraction lines crossing the island in north-south and east-west directions to be used as 2-D profiles; and (3) easily accessible site locations with low noise due to human interference wherever possible.

[20] The quality of the recorded data is generally high and first breaks can be identified up to 30–40 km offset and in some cases up to 60 km. For this study we used data from 125 sites, where the signal-to-noise ratio was high. Corresponding time windows for all the shots were extracted from the continuous wavefronts and the waveforms were filtered using a band-pass zero-phase filter between 4 and 8 Hz (Figure 3). This frequency band, which is narrower than used for many wide-angle crustal-scale studies in other places, was chosen after several tests to maximize the signal-to-noise ratio. For frequencies lower than 4 Hz, the ocean microseisms are masking the signal for larger offsets. For frequencies above 8 Hz, the human-generated noise caused by the high population density strongly perturbs the seismograms. Figure 3 shows filtered seismic signals panels recorded at two stations in the TOM-TEIDEVS experiment. Figure 3a shows a line along the SE coast and recorded at station located at Las Cañadas. Figure 3b shows a NE to NW line recorded at a station located at the SE end of the island. In addition to travel times we also determined a quality factor for each arrival, which varied from 1 (good signal/noise ratio) (quality factor 1 assigned to Figure 3a and quality factor 2 to Figure 3b) to 4 (impossible to distinguish the signal from the noise). Our data set consists of 511,599 P wave first arrival travel times. To perform the inversion we selected only travel times with quality factors 1 and 2 recorded on 125 sites, making for a total of 103,750 travel times. Travel times with quality factor 3 or 4 were not used. Based on our manual

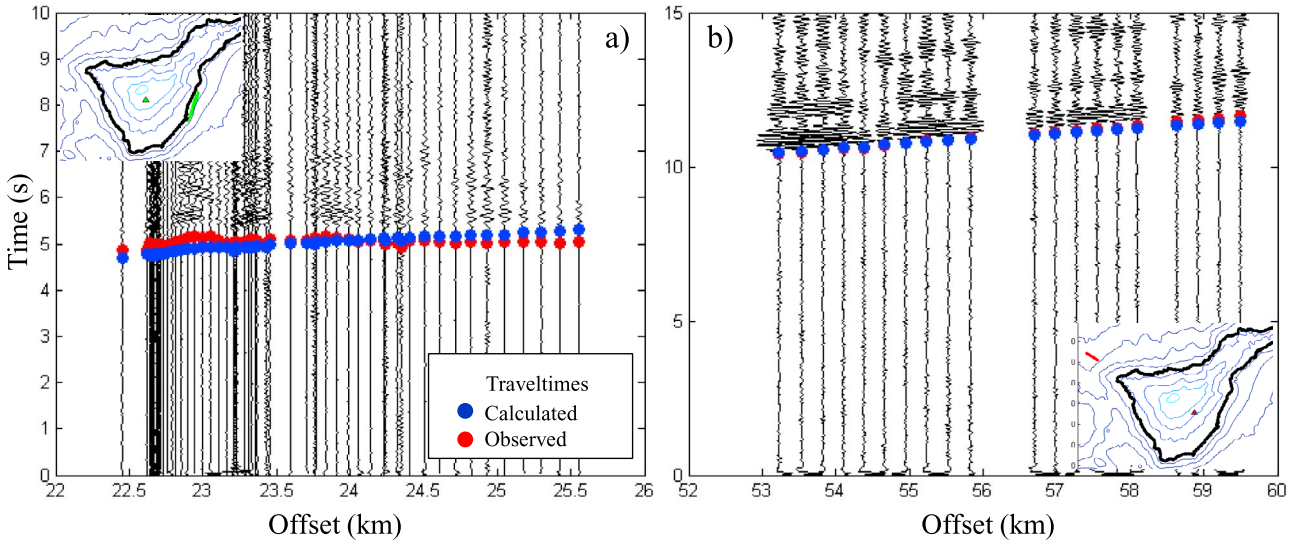

Figure 3. Seismic signals panels recorded at two stations in the TOM-TEIDEVS experiment. The observed traveltimes are in red; calculated traveltimes through the final model are displayed in blue. (a) Line along the SE coast and recorded at station located at Las Cañadas. The quality factor assigned is 1. (b) NE to NW line recorded at station located at the SE of the island. The quality factor assigned is 2.

determination of arrival times, standard errors of +−100 ms and +−150 ms were assigned to the travel time picks with quality factor 1 and 2 respectively.

3.2. Algorithm

[21] In this study we used the inversion program ATOM-3D (Active Tomography in 3D), which was adapted from the passive source tomography program, LOTOS [*Koulakov*, 2009] for the case of 3D active source observations. The inversion uses in general a similar workflow as in some previously developed codes (e.g., FAST code by *Zelt and Barton* [1998]). A detailed comparison can be found in *García-Yeguas* [2010] between ATOM-3D and FAST. Although the results of the inversion provided by both approaches are similar, the ATOM-3D code appears to be more versatile and faster, and was therefore selected for this study. For example, a full inversion cycle including five iterations for 100000 rays takes only about one hour of computing time on a regular PC, while FAST processes the same amount of data for 5–6 h (approx.).

[22] ATOM-3D uses first arrival travel time data as input and provides the 3D distribution of absolute P wave velocity by means of iterative inversions and 3D ray tracing in the updated model. In the case of marine observations, as in this study, the sources (air gun shots) are located on the sea surface. In the first iteration, we traced the intersection of each ray with the seafloor and corrected the travel times for the water column. In following iterations, we performed ray tracing between the points on the sea bottom (Xs, Ys, Zs) and stations (Xr, Yr, Zr) in the updated 3D velocity model using a ray bending method described in *Koulakov* [2009].

[23] The parameterization is performed with a set of nodes distributed on vertical lines regularly spaced in map view (1 km spacing in this case). In the vertical direction the position of the top node is defined by the topography. The distance between nodes depends on the density of rays, yet cannot be smaller than a predefined minimal value (here, 0.5 km). No nodes are installed in areas with insufficient rays (in our case a ray density less than 10% with respect to the average value). In areas between nodes, the velocity distribution is linearly interpolated. In order to reduce the influence of parameterization on the results, the inversion is repeated using several grid configurations with different basic orientations (e.g., 0°, 22°, 45° and 67°) and subsequently averaged. This model is then used as the basic velocity distribution for the next iteration. The parameterization grids are constructed in the first iteration; in subsequent iterations, velocity values are updated for the same nodes.

[24] During each iteration, partial derivatives are computed along the raypaths in the current velocity model. The inversion of this matrix, which consists in minimization of the root mean square of residuals (difference between the observed and modeled travel times), is performed using the LSQR method [*Paige and Saunders*, 1982; *van der Sluis and van der Vorst*, 1987]. The amplitude and smoothness of the solution are controlled by two additional matrix blocks, whose weights play an important role in tuning the resulting model. However, for finding the optimal balance between the inversion and damping values there is no any formal criterion, and we estimated their values using synthetic modeling (see synthetic test with realistic patterns in section A3).

[25] After computing an updated velocity model we repeat the steps of ray tracing, matrix calculation and inversion. This iterative procedure was done several times, reducing the nonlinear effect due to dependency of the raypaths on the unknown velocity distribution. Increasing the number of iterations has an effect similar to reducing the damping value. Therefore, to find the optimum properties of the solution, we fixed the number of iterations and tuned the damping values; 5 iterations is a compromise between reduction of the nonlinear effect and the time of calculations.

4. Results

[26] Based on our data selection and inversion strategy we obtained a three-dimensional (3D) P wave velocity model

beneath Tenerife Island. To assess the reliability of the obtained model we performed several tests which are presented in appendices 1 to 3. In particular, the role of the starting 1D model and inversion parameters were explored by several inversion trials with different starting conditions (inversion parameters and starting models) (section A1). The quality of data and the role of random noise were tested using a jackknife test (section A2). The spatial resolution was estimated using a series of synthetic models (section A3). In particular, the test with realistic anomalies, which mimics the conditions of the real experiment (same inversion parameters and reference model), was used to estimate the optimum value of damping and number of iterations. It shows that the considerable magnitude of anomalies (up to 40%) can be retrieved robustly with the chosen inversion scheme. As follows from the tests, reliable images were obtained beneath the entire Island at a depth range from the top of Teide volcano (over 3000 m a.s.l.) to a depth of 8000 m b.s.l.

[27] The results are shown in vertical cross-sections and in horizontal sections at different depths in absolute P wave velocity and percentage deviation from a 1D starting model. Note that for the offshore parts, where the rays do not intersect sufficiently, the results are strongly smeared. Therefore, in our further interpretation we only consider the onshore parts of the model covering an area of about 40 × 40 km2.

[28] Vertical and horizontal cross-sections through the final tomographic model are shown in Figure 4–7: a N-S section (Figure 4a), a W-S section (Figure 4b), an oblique NW-SE section (Figure 4c) and horizontal sections at different depths (Figures 5 and 6). Figure 7 shows in detail the CTPVC region for horizontal sections at different depths. The P wave velocity distribution is highly heterogeneous with very large contrasts, reaching a maximum of +−40% in some areas particularly close to the surface (between 3 km a.s.l. and 3 km b.s.l). The most significant anomalies are marked with numbers and section letters in Figures 4 and 6 (positive anomalies marked with a P and negative anomalies with an N) and are discussed below.

[29] *CTPVC*: The volume situated beneath CTPVC mainly presents high (defined as higher than the average 1D starting model) P wave velocity (∼+22%, with maxima of up to ∼+35%). Lower P wave velocities are observed North-East of CTPVC, corresponding to anomaly N6 (Figures 4b and 4c), showing low P wave velocity (∼−16%) from the top to a depth of around 500 m b.s.l.

[30] At large depths, a high P wave velocity core characterizes the central structure of Tenerife Island in general. This high P wave velocity core, reaches the surface in CTPVC.

[31] *Negative anomalies around CTPVC:* North of the CTPVC there are two low P wave velocity bodies, N2 (Figure 4a), at a depth of around 1 km (b.s.l). Low P wave velocity bodies appear in other areas toward the South and East of the island, namely, anomalies N4 (∼2 km (b.s.l.)) N1 (∼2 km (b.s.l.)) and N7 (∼3 km (b.s.l.)) (Figure 4). The regions surrounding the anomalies N5 (∼7 km (b.s.l.)) N1 (Figure 4) are low P wave velocity areas.

[32] In depth, the low P wave velocity anomalies are mainly distributed around the high P wave velocity central structure, except for anomaly N4, surrounded by high P wave velocity. With decreasing depth, the low P wave velocity anomalies increase in size and amplitude, taking up more central positions in the island; anomaly N4 follows the same pattern.

[33] *Positive anomalies around CTPVC*: In general, the high P wave velocity anomalies (P1 (Figure 4a), P5 (Figure 4b) or P10–P11 (Figure 4c)) reach the depth of the tomography image resolution at, 8, 10 and 11 km (b.s.l.), respectively.

[34] *Anomaly contrasts and volcanic eruptions distribution*: There is no preferential orientation or alignment of P wave velocity anomalies. We also note that in some regions there is no continuity in the anomalies from the surface to the bottom of the model. For example the negative anomaly N3 becomes positive at the surface, north of anomaly P9. In contrast for example the positive anomaly P6 at depth is reversed into a negative anomaly N1 at the surface.

5. Discussion

5.1. Main Features of Tenerife Tomography Model

[35] Tenerife Island is characterized by a high P wave velocity core (Figure 6). This feature is typical of most stratovolcanoes and oceanic islands, including Etna [*Aloisi et al.*, 2002], Vesuvius [*Di Stefano and Chiarabba*, 2002], Asama [*Aoki et al.*, 2009], and Montserrat [*Paulatto et al.*, 2010, 2012; *Shalev et al.*, 2010].

[36] In the central massif we find the highest positive P wave velocity contrast of the entire island, anomaly P3, at the Boca Tauce volcano (Figure 6). Surface geological studies report that this area is old and highly eroded [*Martí et al.*, 1994]. This edifice probably represents the oldest stratovolcanic formation in the CTPVC. We therefore infer that this area may represent the point where the basal complex started, forming along with the large structure of CTPVC. This observation is in line with other geophysical studies: *Canales et al.* [2000] describe a high P wave velocity anomaly in this area using active seismic data; and *Araña et al.* [2000] and *Gottsmann et al.* [2008], through gravimetric studies, observed a high density core in the CTPVC and emphasizing Boca Tauce volcano.

[37] Our tomographic model shows a high P wave velocity anomaly at the center of Tenerife Island without any clear preferred orientation at any depth, which could be associated with an old rift structure. Therefore, our results do not support the evolution models of Tenerife Island which postulates that the joint action of the three rifts conditioned the volcanic activity of Tenerife. Many authors [i.e., *Carracedo et al.*, 2009] hypothesize the existence of these three rifts on the basis of surface morphology. Yet there is no general agreement on this issue. Our tomographic image shows a high velocity central body surrounded mainly by low velocity anomalies and similar velocity abnormalities have been observed in other active volcanic islands such as Montserrat [*Shalev et al.*, 2010].

Figure 4. Results of experimental data inversion (final model) with vertical sections. (left) Relative perturbations with respect to the 1D reference model; (right) absolute velocities. Locations of the profiles are given in the map in the upper-right corner. Letters P and N indicate the positive and negative anomalies which are discussed in the text. The arrows indicate where the anomaly is located.

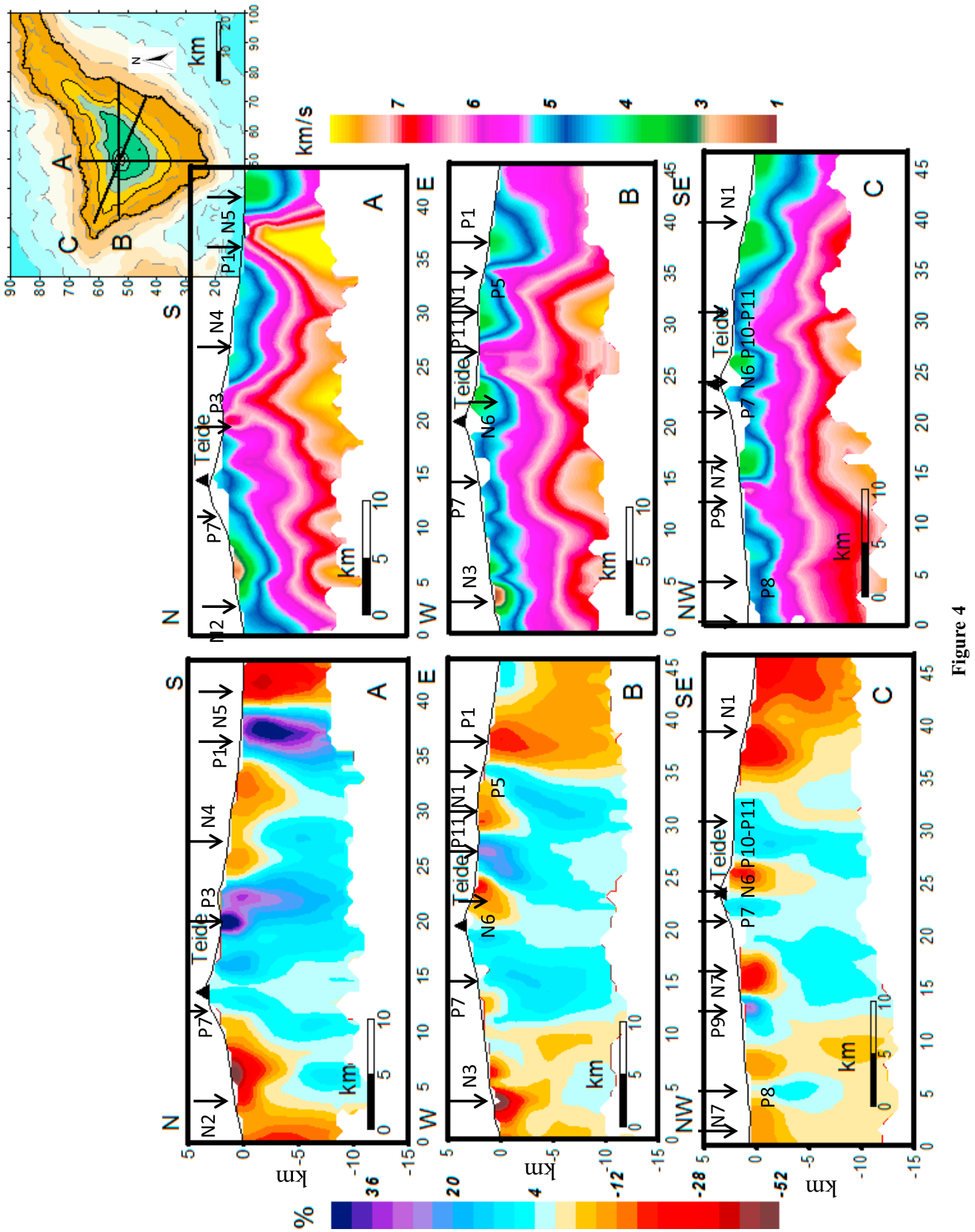
A
B
C
km
km/s
%
Teide
N1
N2
N3
N4
N5
N6
N7
P1
P3
P5
P7
P8
P9
P10-P11
N
S
W
E
NW
SE

Figure 4

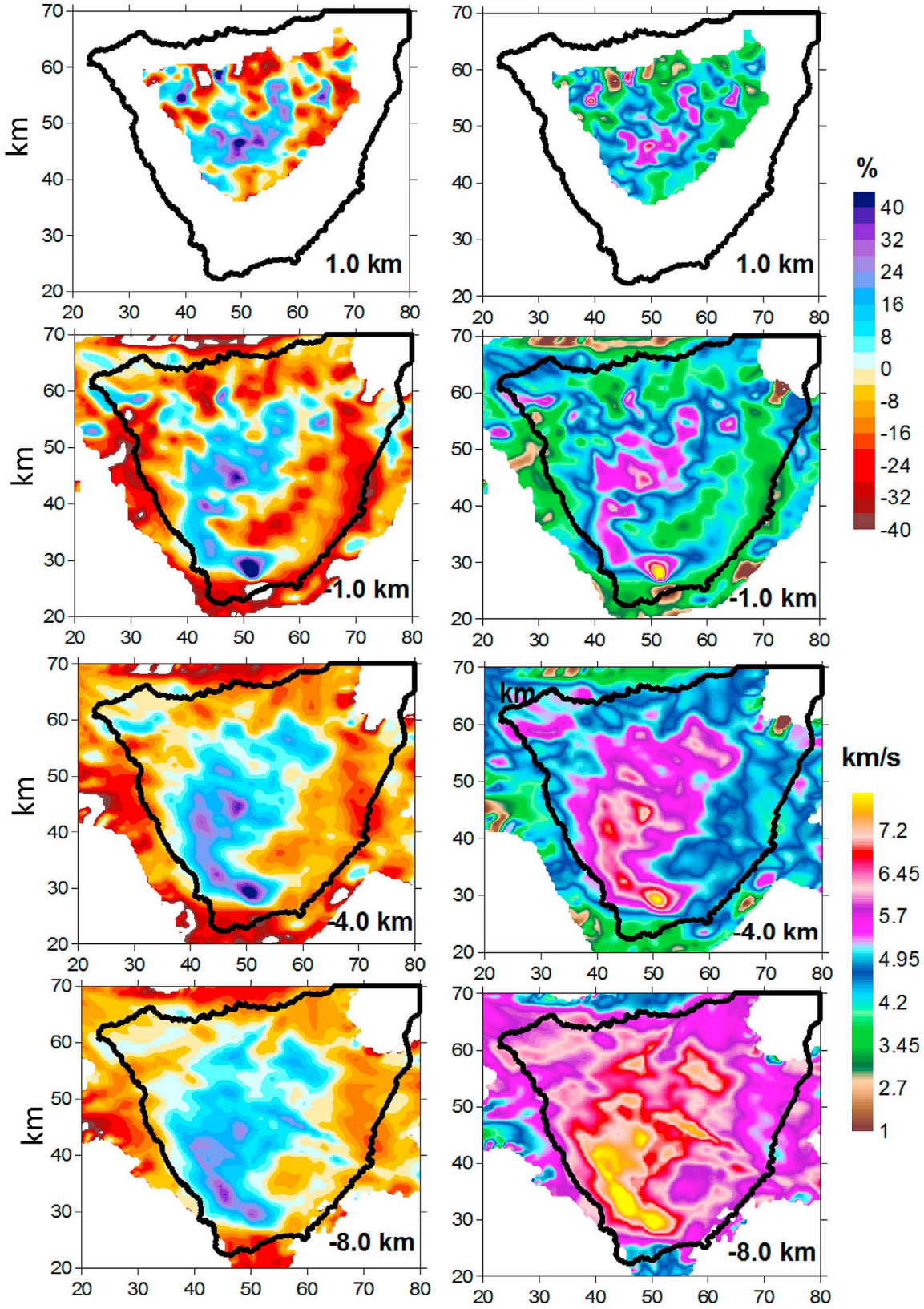

Figure 5. Results of experimental data inversion with horizontal sections. (left) Relative perturbations in respect to the 1D reference model; (right) absolute velocities. Depths are given in respect to sea level. The results are masked in areas where the distance to the nearest parameterization node in more than 3 km.

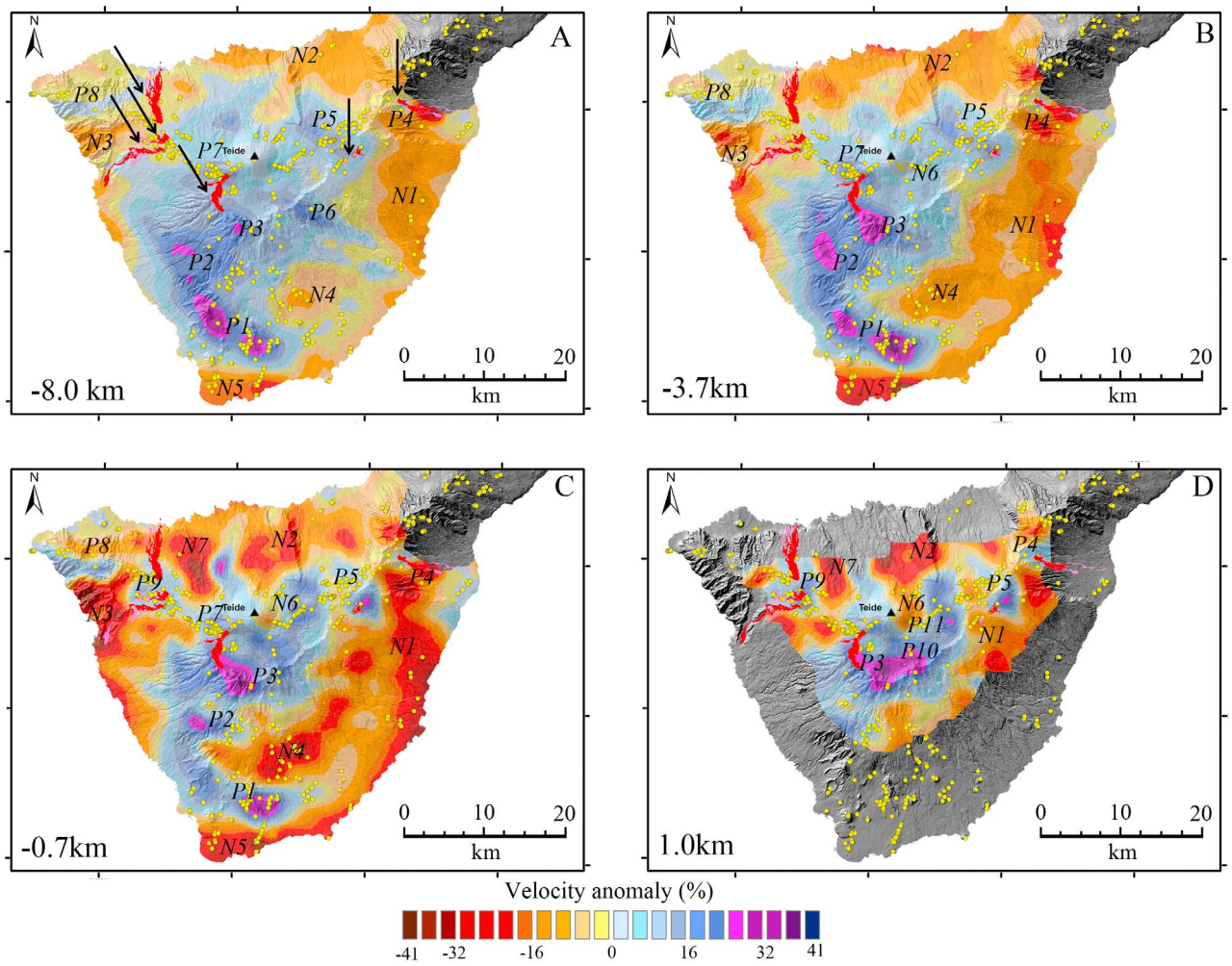

Figure 6. Horizontal sections at different depths for final model with indications of structural features discussed in the text: (a) −8.0 km, (b): −3.7 km, (c) −0.7 km and (d) +1.0 km. The yellow dots represent the volcanic eruptions emission visible at the surface today centers. The red areas (indicated by arrows) pertain to historical eruptions. Letters P and N with numbers indicate the positive and negative anomalies discussed in the text. The results are masked in areas where the distance to the nearest parameterization node in more than 3 km.

[38] On the island of Tenerife we found varying velocity contrasts, up to 40% with reference to the initial model. It is not surprising to find such contrasts in volcanic regions. For example, *Shalev et al.* [2010] in their study of Montserrat, using a similar tomography technique found velocity contrasts of 20% within a distance of less than 5 km and in a study region four times smaller than Tenerife.

5.2. The Nature of the Las Cañadas Caldera and the Presence or Absence of an Active Magma Chamber

[39] At present, the debate about the origin of the Las Cañadas caldera is dominated by two main theories: collapse caldera [*Martí et al.*, 1997] or landslide models [*Masson et al.*, 2002]. The resolution of our seismic tomography images of Tenerife Island, while high, cannot accurately determine specific events. A distinct body with high P wave velocity at depth is associated with the basal complex, and another high P wave velocity body is associated with the stratovolcanic structure. Accordingly, it is interpreted to be related to the system's evolution, growth and consolidation.

[40] Our images do not permit conclusions as to whether the current state of the Cañadas is due to a collapse process or a large avalanche. In either case, the large volume of surface material would have been deposited out at sea. The absence of a surface layer of low P wave velocity in the structure of CTPVC implies that there are no substantial volcanoclastic deposits in the highly fractured area or significant material strength. In this context, we might envisage a process of regional emptying; the collapse process would entail fractured amorphous volume with sufficient velocity and small thickness of the deposit layers.

[41] It is noteworthy that our observations do not offer a clear indication of a low velocity region that could be associated with a magma reservoir. The existence of a magma chamber with a size under $3 \times 3 \times 3$ km volume (the resolution of our model) cannot be ruled out base on our tests.

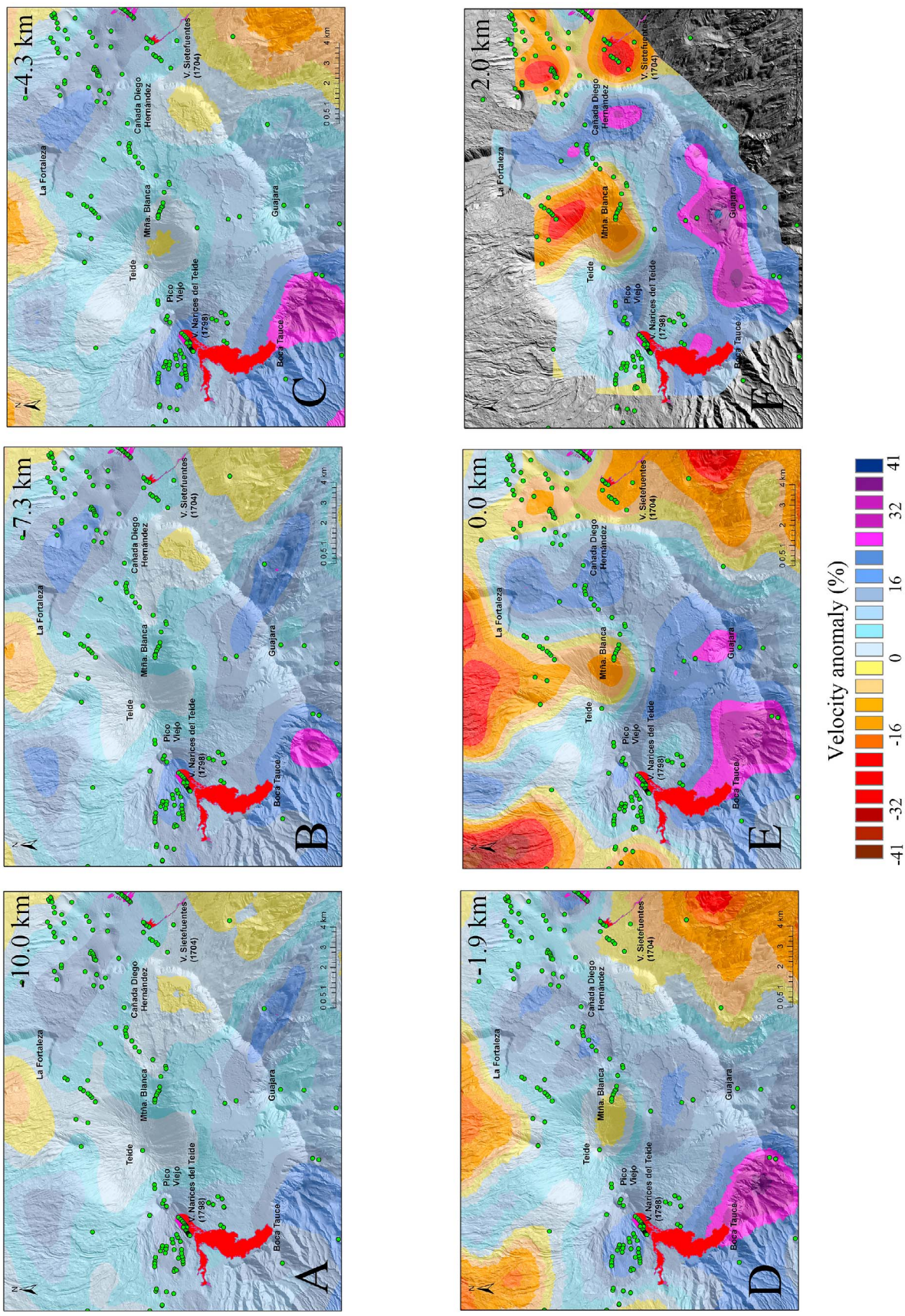

Figure 7. Horizontal sections of P-velocity anomalies at different depths for final model overlapped with the shaded relief in the area of CTPVC: (a) −10.0 km, (b) −7.3 km, (c) −4.3 km, (d) −1.9 km, (e) 0.0 km, and (f) 2.0 km. Green dots represent the volcanic eruptions centers. The red area indicates the historical eruption of La Chahorra (1798).

[42] The main volcanic structure is the complex of CTPVC (Figures 1 and 7). Although only one historical effusive eruption occurred inside this region (eruption of 1798 [*Romero*, 1992]), it was formed by several highly explosive episodes related to Plinian eruptions [*Ablay et al.*, 1995]. Additionally, the evolution theories of this complex include collapse caldera episodes [*Martí et al.*, 1997; *Martí and Gudmundsson*, 2000] or enormous landslides [*Masson et al.*, 2002; *Blanco-Montenegro et al.*, 2011]. The tomographic images of this area are shown in Figure 7 lead us to remark on the following features:

[43] 1. There is no evidence of shallow low-seismic-velocity layers within the caldera that would correspond to soft volcanoclastic deposits. On the other hand, based on the resolution tests, it could be is difficult to detect.

[44] 2. A remarkable but small vertical low-seismic-velocity structure, extending from the surface to about 3000 m b.s.l (Figures 4b, 4c and 6, anomaly N6), is observed beneath Montaña Blanca, a monogenetic cone produced by a Plinian eruption 2000 years ago. Previous authors such as *Araña et al.* [2000] and *Gottsmann et al.* [2008] observed a similar anomaly in gravimetric models, yet located beneath Teide volcano, to the west of our observations. They associated this anomaly to hydrothermal alteration, since the Teide summit has some fumarolic activity [*Pérez et al.*, 1996]. In our case such and interpretation may also be valid.

[45] 3. There is a clear relationship between the values of maximum high P wave velocity anomalies and the evolution model of the CTPVC. *Ancochea et al.* [1990] postulated an evolution model that migrates from South to Northwest (present position of Teide volcano) producing different calderic formations. The places cited by these authors harbor the main emission centers, where we observe maximum values of P wave velocity anomalies. Presently and at the surface, these centers are marked by several frozen dike swarm intrusions and magmatic bodies, confirming our high P wave velocity values and supporting the model of frozen plutonic intrusions at depth as responsible for the high P wave velocity anomalies.

5.3. Other Seismic Velocity Anomalies and Their Relation to Old and Recent Volcanism

[46] The central body of high P wave velocity is surrounded by several areas with low P wave velocity anomalies producing high horizontal P wave velocity gradients. The largest low P wave velocity region is located in the Eastern part of Tenerife island (anomaly N2), but other considerable regions are observed in the North (Orotava valley) and on the western coast of the island (anomaly N3). All are present from the surface to the maximum imaged depth of resolution (around 10 km b.s.l.). The lowest anomaly, with contrast under 40%, is observed beneath La Orotava valley. In general, all these low P wave velocity bodies increase in size closer to the surface, where also the lowest P wave velocity values are reached.

[47] The interpretation of these bodies is complex. Possible explanations are the presence of fluids in the medium (water, gas or magma), highly fractured or porous rocks, hydrothermal alterations, volcaniclastic deposits, landslide deposits, or combinations of these. Moreover, different interpretations can be envisaged for the same body at different depths.

[48] The deeper regions surrounding the high P wave velocity central massif can be attributed to ancient volcanoclastic deposits or an alteration of the original island processes due to interaction with water. As we approach the surface, the low P wave velocity contrast is more evident.

[49] One of the most interesting observations of our work is the existence of velocity anomalies in small areas surrounding the central body. In particular, we highlight the regions observed for historical volcanism, where we detected the existence of high P wave velocity bodies above deep low P wave velocity bodies. Given the strong correlation between these regions and their recent volcanism, we suggest that these anomalies trace systems involving magmatic intrusion; high P wave velocity at the surface is associated with cooled magma, while low P wave velocity indicates the existence of a deep magmatic body responsible for the rash that has not yet cooled.

[50] The upper most layers along the NW ridge, where some of the last historic volcanic eruptions occurred (Boca Cangrejo, 1492; Garachico, 1706; Chinyero, 1909) are characterized by high P wave velocity gradients (P9 positive anomaly). However, at around 3 km b.s.l. a strong low P wave velocity perturbation is observed (Northeast of N3 negative anomaly).

[51] We interpret this structure as a consequence of the observed historical eruptions. The low P wave velocity of the lower layer is conditioned by remaining magma body intrusion, still hot, and located in a weak external region.

[52] Some external areas of Tenerife Island have vertical gradients showing low P wave velocity anomalies at the surface and high P wave velocity at greater depth. The high P wave velocity is clearly related to the basal complex of the first formation stage of the island. The low P wave velocity anomalies may be a result of highly fractured regions, hydrothermal activity and/or large volcanoclastic deposits. However, there is a noteworthy zone in the southern part of the island (N4 in Figure 6) where additional observation could modify this interpretation. *Pérez et al.* [1996] observed an anomalous ratio He3/He4 precisely in this region. This ratio is a clear marker of the presence of magma at depth beneath this area. Hence, the low P wave velocity anomaly in the area of N4 might also be interpreted as the consequence of magma.

6. Conclusions

[53] This paper presents the results of a 3D seismic P wave velocity tomography study of Tenerife Island using active source data. Our images were obtained using travel times of 103,750 P waves' first arrivals, recorded at 125 locations. The maximum depth resolved is about 13 km, from the top of Teide summit down to 10 km b.s.l. The horizontal resolution covers the total subaerial part of the island except the Northeast region.

[54] The results of tomography shed light on the evolution of the island's formation processes, pointing to the region where the initial or basal stage most likely started.

[55] 1. Evidences of a magma reservoir: There is no evidence of a large low-seismic-velocity anomaly beneath Teide volcano that could be interpreted as an active magma chamber. Furthermore, a small low P wave velocity region in this complex is possibly related to hydrothermal alteration. The resolution of seismic tomography images of Tenerife Island, though high, does not suffice to accurately determine

Table A1. Different Starting Models With Their Initial and Final RMS

Depth (km)	Model A	Model B	Model C	Model D	Model E	Model F
3.0	4.3	4.0	4.3	4.0	4.6	4.1
−2.6	5.9	5.6	5.6	5.0	5.5	5.5
−6.6	6.8	6.5	6.5	6.0	6.5	6.5
−11.4	8.0	7.5	7.5	7.0	7.5	7.2
−16.4	8.1	7.9	7.9	7.5	8.1	8.0
−30.0	8.2	8.2	8.2	8.0	8.3	8.2
RMS initial (ms)	875.0	719.3	749.7	619.3	756.0	699.0
RMS final (ms)	189.0	187.8	187.9	187.0	189.0	187.8

the existence of a magmatic chamber with a size less than 3 × 3 × 3 km.

[56] 2. Vertical collapse versus giant landslide: The fact that our inversion cells were 1 × 1 ×1 km3 means only larger structures can reliably be detected. In this sense, our tomographic images do not elucidate the evolution of the CTPVC. Our images are not conclusive as to whether the current state of CTPVC is due to a collapse process or a large avalanche. However, the absence of a surface layer of low P wave velocity in the structure of CTPVC suggests there are no substantial volcanoclastic deposits in the area or highly fractured material of significant strength. Such a scenario would be more compatible with a process of regional emptying rather than a collapse process.

[57] 3. Evidences of the basal complex: We observed a high P wave velocity body at depth that is associated with the basal complex, and a further high P wave velocity body associated with the stratovolcanic structure. This central high P wave velocity body can be interpreted as an evident of a model formation of the island arising from a single central volcanic source. In other stratovolcanoes, such high velocity bodies have been interpreted as evidence of the system's evolution, growth and consolidation.

[58] 4. Structure of CTPVC: The main volcanic structure of the CTPVC is characterized by a high P wave velocity body, similar to many other stratovolcanoes. The presence of different high P wave velocity maxima inside this complex may be related to the geological and volcanological evolution of the system. Our images are not conclusive as to whether the current state of CTPVC is due to a collapse process or a large avalanche. However, the absence of a surface layer of low P wave velocity in the structure of CTPVC suggests there are no substantial volcaniclastic deposits in the area or highly fractured material of significant strength. Such a scenario would be more compatible with a process of regional emptying rather than a collapse process.

[59] 5. External regions of Tenerife Island: In the external regions of Tenerife Island, a few low P wave velocity regions can be interpreted as fractured zones, hydrothermal alterations, porous materials, thick volcanoclastic deposits or their combination.

[60] Our images reveal a complex structure of Tenerife Island, with strong P wave velocity gradients associated with different volcanic processes involved in its evolution. The low P wave velocity regions at the external areas surrounding a high P wave velocity core (CTPVC) can be interpreted as "soft" regions, and it is remarkable that recent historical eruptions took place precisely in these surrounding regions.

Appendix A: Verification of the Results

A1. Effect of the Reference Model

[61] The ATOM-3D code requires using 1D starting models which is estimated by minimizing the difference between the observed and modeled travel times [e.g., *Sallarès et al.*, 2003]. To evaluate the effect of the starting models upon the final velocity distribution we have performed a series of inversions for different 1D starting velocity models. In Table A1 we present six different reference velocity models with considerably different 1D velocity distributions. In the same table we present the values of RMS of residual after tracing in the initial and final models. It can be seen that the RMS in the first iteration are considerably different for different models. After five iterations of inversion, the difference in RMS becomes much smaller. In Figure A1 we present the resulting absolute velocities for models A and F with considerable differences in reference models. The two starting models result in similar relative perturbations but slightly different absolute velocities. It shows that the present observation scheme cannot give strong constraints on the absolute velocities, but is rather robust with respect to the anomalies. This means that we should be careful about interpreting the absolute velocities and mostly concentrate on consideration of relative heterogeneities.

A2. Effect of Inversion Parameters

[62] Having chosen the initial model, we proceeded to select the inversion parameters, the smoothing parameter and the value of the amplitude of damping. Figure A2 plots different inversion images, at 3 km of depth, for various values of the parameters. When determining the optimal smoothing coefficient, we tried to avoid both excessively patchy structures caused by low damping and oversmoothed solutions. The optimal values were fixed using synthetic modeling (see section A4). Table A2 shows the values of the final RMS obtained for the four models after 5 iterations plotted in Figure A2. Although model A provided the lowest RMS, we adopted the parameter combination of model D since it proved robust, low in RMS value, and capable of providing realistic P wave velocity contrasts. The final RMS varies after each iteration as: 630.37 ms (iteration 1), 515.57 ms (iteration 2), 235.58 ms (iteration 3), 198.74 ms (iteration 4), 187.72 ms (iteration 5).

A3. Jackknifing Test

[63] We randomly removed 25% and 50% of the seismic stations and inverted the data again to obtain a P wave velocity model without all the data. Figure A3 shows the models derived with the full data set and using the reduced data set. The fact that there are no great differences is evidence that the random noise in the data does not strongly affect the results. At the very south tip of the island along the NS station line there is a significant difference: In the inversion with all stations there is a strong contrast between low velocities on the coast and high velocities inland, but the contrast becomes much smaller with 75% and 50% of the stations. This suggests some inconsistency between some of the stations, perhaps because of high relief which cannot be properly accounted for with the 1 km grid.

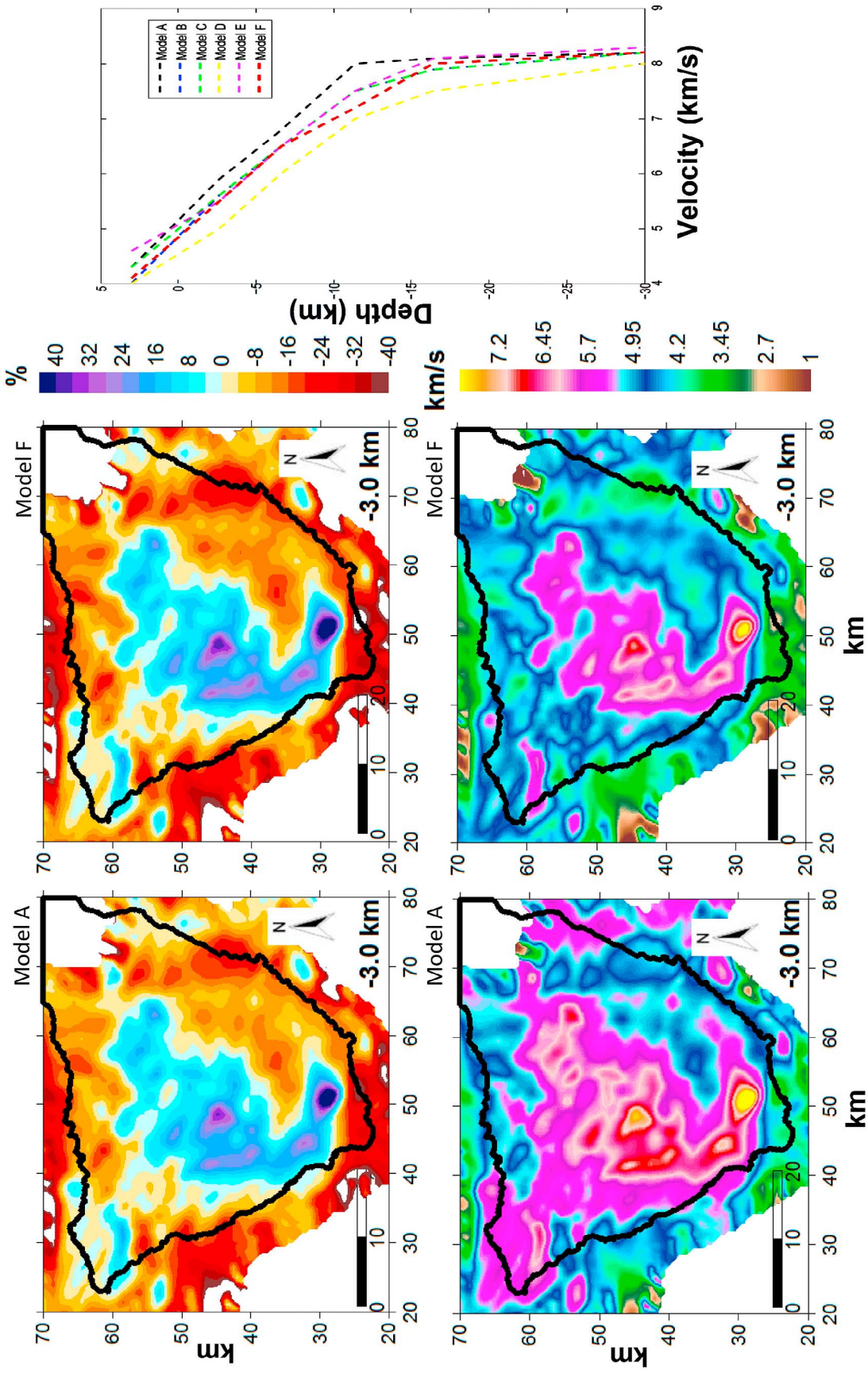

Figure A1. Results of inversions with two different reference models. (left, middle) The inversion results are shown for the models A and F. Top row shows anomalies, while bottom row shows absolute velocities. (right) Various reference models used for the testing and described in Table A1.

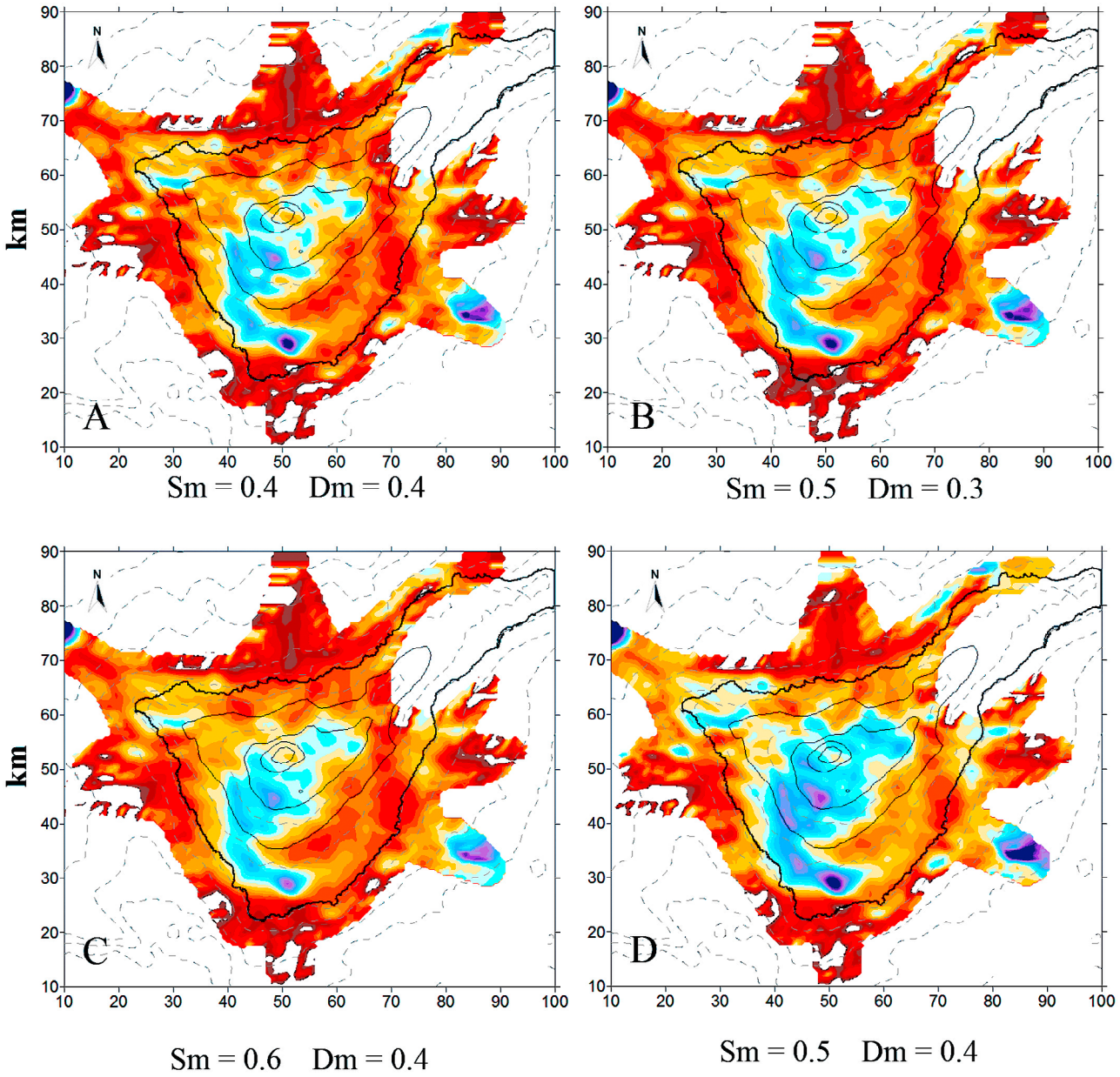

Figure A2. P-velocity anomalies at −3.0 km depth derived after the inversion with different free parameters indicated on each plot. Thin solid and dotted lines depict topography and bathymetry contours.

A4. Synthetic Tests

[64] Here we present several synthetic tests which were performed, first, to estimate the optimal values of the inversion parameters, and, second, to access the spatial resolution of the retrieved model. In all tests, the synthetic travel times were computed between same source-receiver pairs as in the field experiment using the bending ray tracing algorithm [*Koulakov*, 2009]. The reconstruction was performed in identical conditions as in the case of real data inversion.

A4.1. Checkerboard Test

[65] Checkerboard test is widely used in many tomographic studies and it consists in reconstruction of periodical alternating anomalies. Performing this test with different sizes of anomalies allows direct showing the capacity of the tomography to resolve certain size of pattern in certain parts of the study area. Here we show the test with anomalies of 5 km by 5 km horizontally and 8 km vertically, with a P wave velocity anomalies varying ±10%. Figure A4 shows the checkerboard input model on the left, and the model after inversion on the right, at different depths (1.0 km, −1.0 km, −4.0 km and −8.0 km). Resolution varies with position and depth. At 1 km a.s.l. the central part of the island is very well resolved. At depths b.s.l. in the South boundary of the island there is some smearing of the recovered anomalies, indicating lower resolution. The center of the island is well resolved for all depths. The resolution of the experiment shows well resolved anomalies in all the selected sections from the surface to a depth over 8 km b.s.l. At surface, the whole island,

Table A2. Pair of Smoothing and Damping Parameters With Their Final RMS

Model	Smoothing	Damping	RMS Final (ms)
A	0.4	0.4	186.16
B	0.5	0.3	187.32
C	0.6	0.4	192.42
D	0.5	0.4	187.72

except for the NW region not covered by seismic stations, is also very well resolved. For the positive anomaly the input value of the anomaly was 10%. In the retrieved model we recovered around 8% of the amplitude. For the negative anomaly, the input value of the anomaly was −10%. In the retrieved model around −6 to −7% was recovered; this value is less than for the positive anomaly, as to be expected.

A4.2. Discrete Anomalies Test

[66] In Figure A5 we present the input P wave velocity anomalies and the reconstruction results in horizontal and vertical sections. We introduced three P wave velocity anomalies: two negative (−15% of the background velocity at that depth) and one positive anomaly (15% of the background velocity at that depth). In the upper part of Figure A2 we show the recovered model at 0.0 km and −5.0 km of depth. Both types of anomalies, positive and negative, were effectively represented. Although authors such as *Flecha et al.* [2004] underline the difficulty of reconstructing low P wave velocity anomalies, our data set provided sufficient

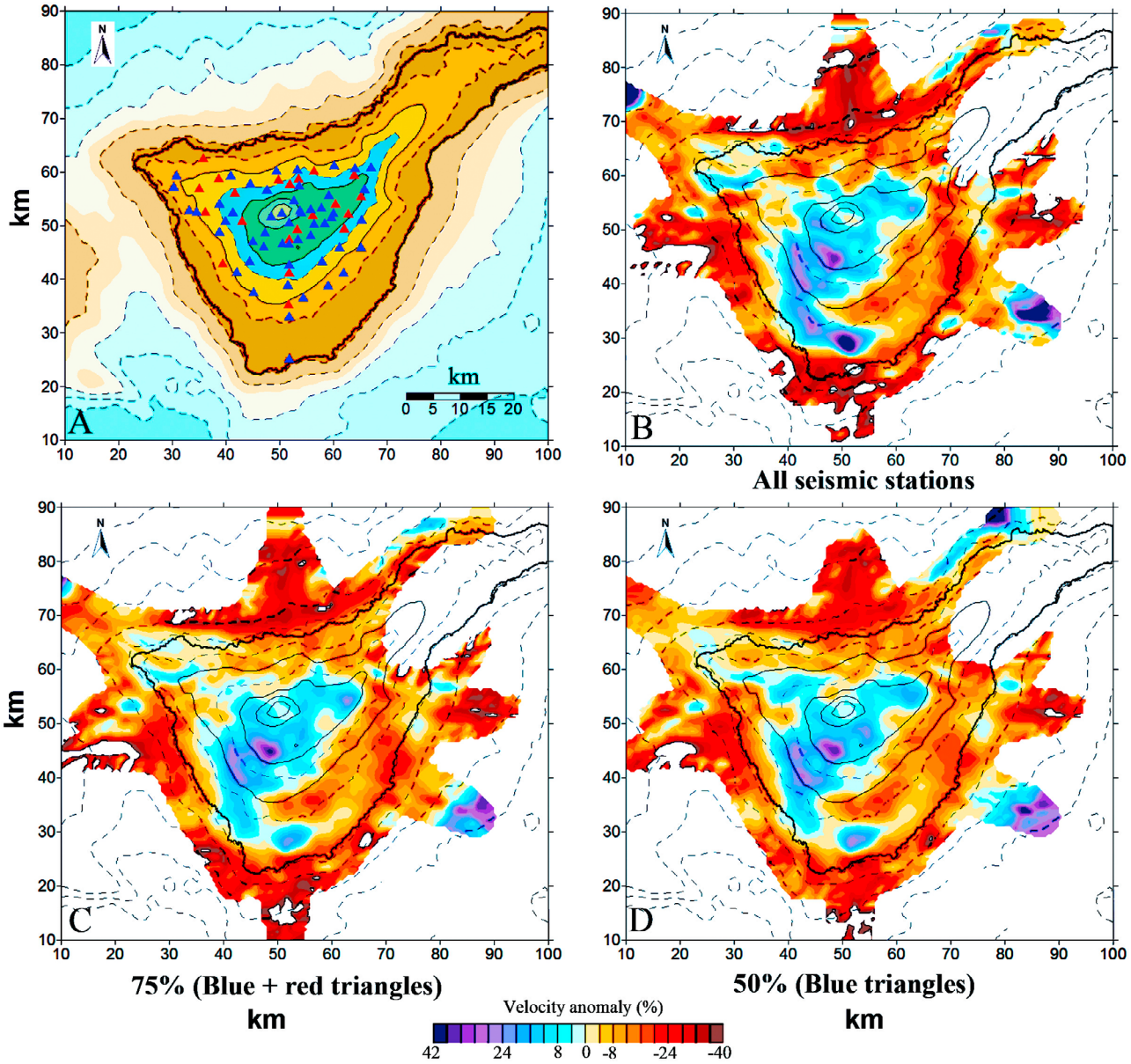

Figure A3. (a) Stations of the network: red stations indicate 25% of stations which were randomly removed to obtain the result in Figure A3c. (b–d) Results of the jackknife test with maps of velocity anomalies at 3 km depth derived after inversions with all data (Figure A3b), with removal of 25% of stations (Figure A3c), and with removal of 50% of stations (Figure A3d).

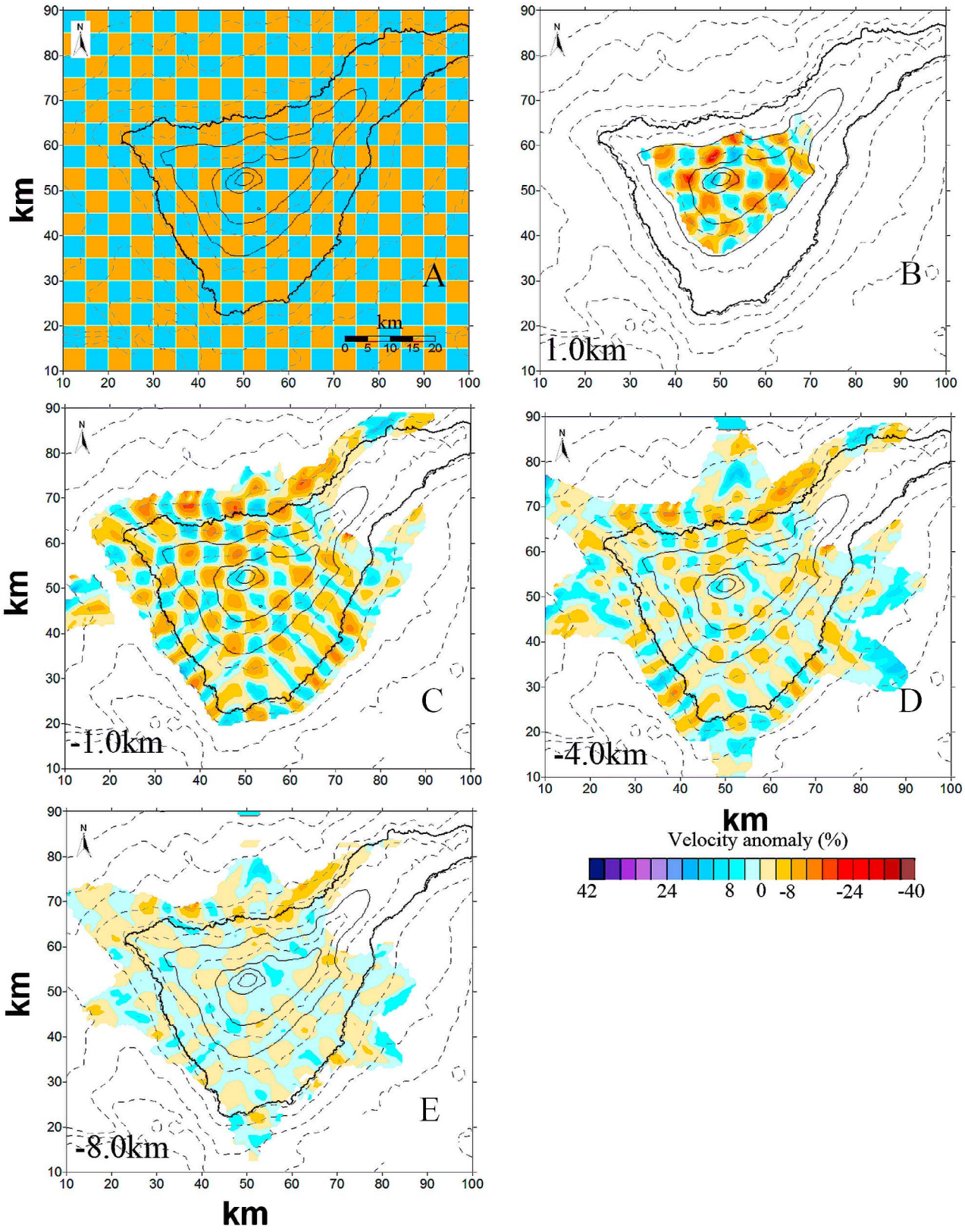

Figure A4. Result of the checkerboard test. (a) The distribution of synthetic anomalies which remain unchanged at all depths. (b–e) The reconstructed velocity anomalies at different depths indicated in the bottom right corner of each plot.

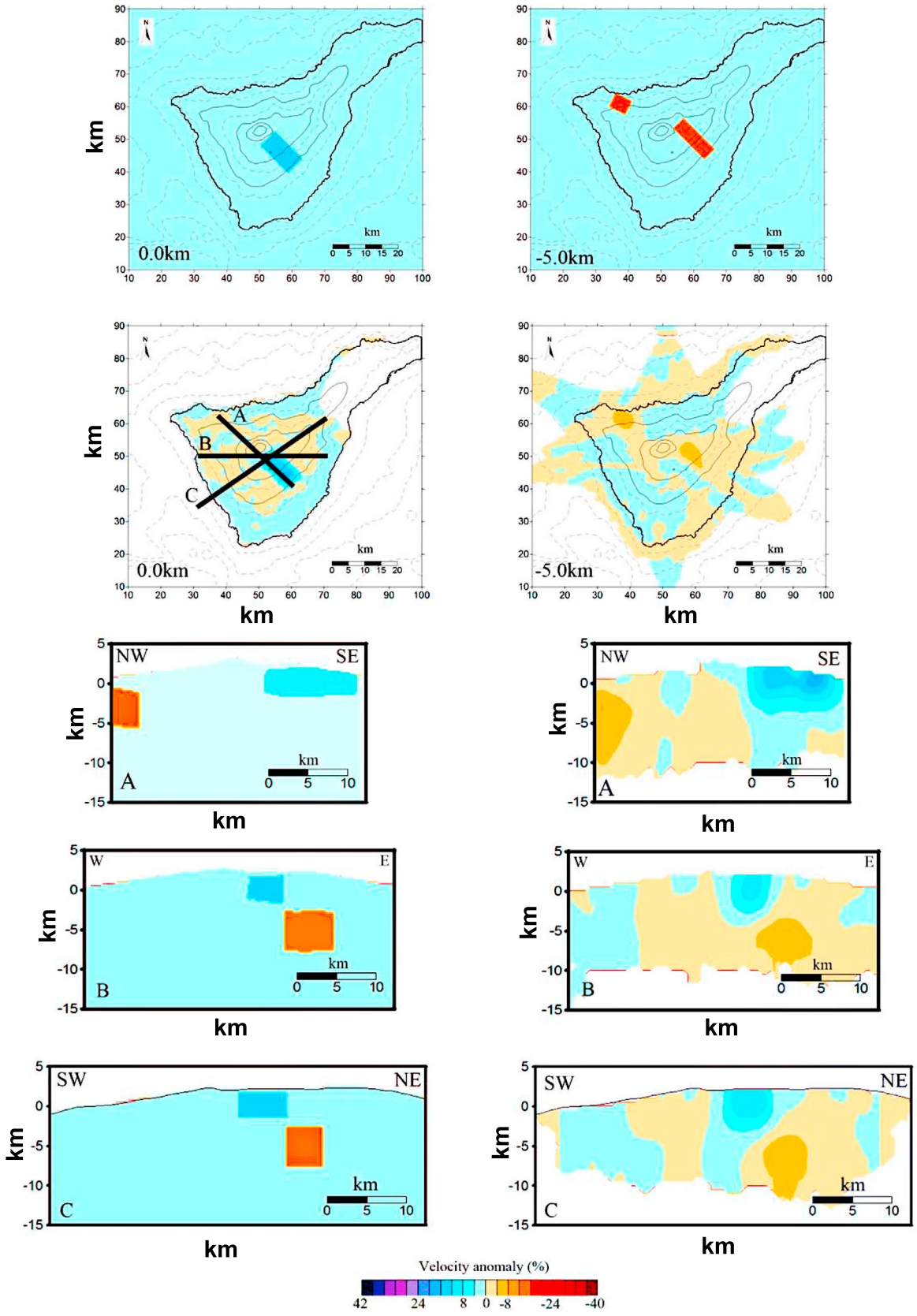

Figure A5. Synthetic test with three discrete anomalies. Top row shows the synthetic anomalies in horizontal sections and second row shows results of reconstruction for the same sections. Lower three rows show synthetic model and reconstruction results in vertical sections (left and right columns, respectively). Location soft the profiles are indicated in one of the maps.

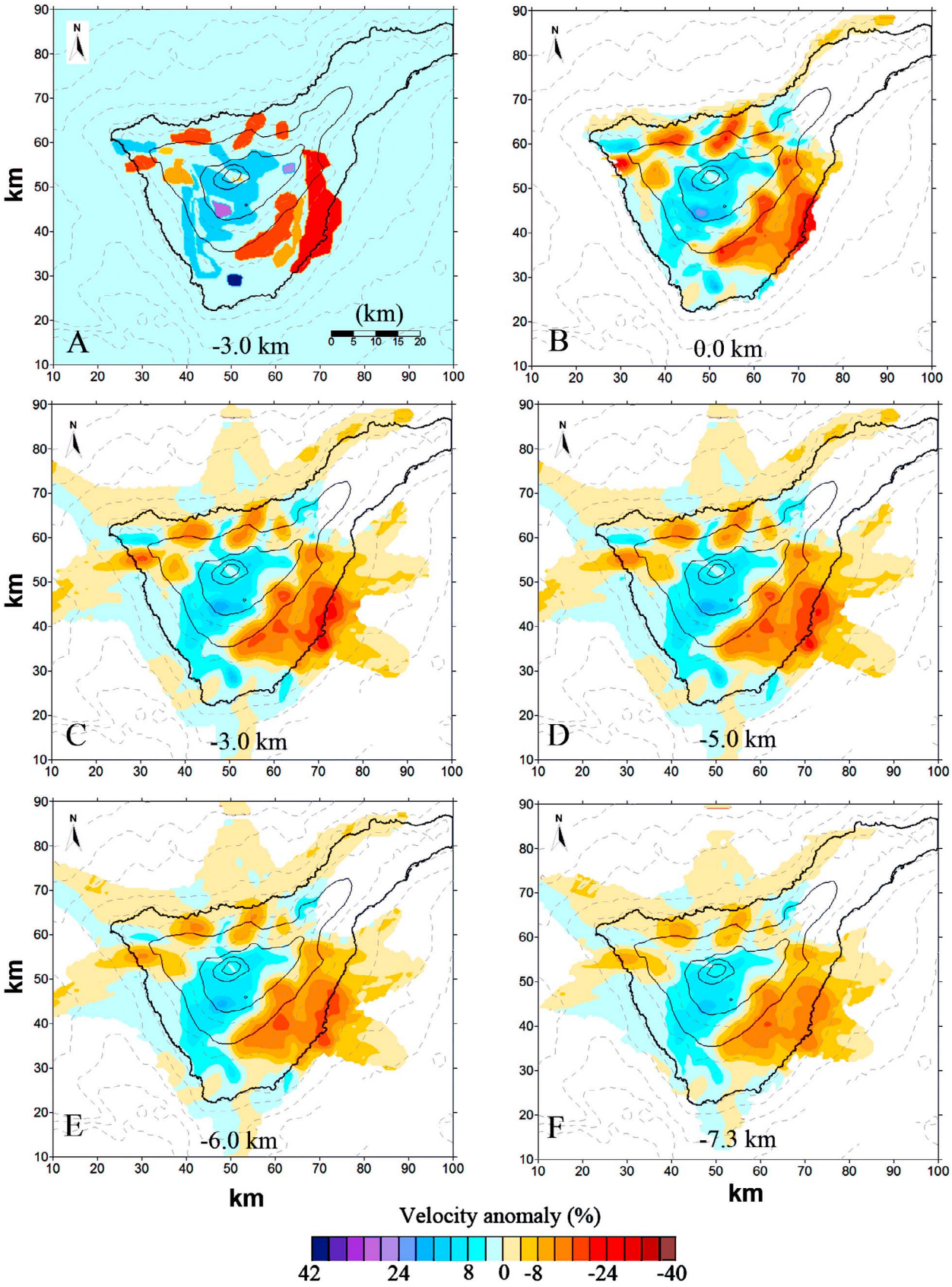

Figure A6. Synthetic test with free-shaped anomalies representing a realistic configuration of seismic velocity patterns. (a) The distribution of synthetic anomalies which remain unchanged at all depths. (b–f) The reconstructed velocity anomalies at different depths indicated in the bottom right corner of each plot.

quality for the return of any type or position of P wave velocity anomalies greater than 15 × 5 × 5 km3 in size. At the bottom of Figure A5 we show the vertical sections with different orientations. On the left are the vertical sections of the input model, and on the right those of the retrieved model. Figure A5a clearly reflects the NW negative anomaly and positive anomaly. In Figures A5b and A5c, meanwhile, we observe the E and SE positive and negative anomalies. The results, aside from confirming the high quality of our data set, demonstrate the capacity of this method for identifying and resolving a high gradient of P wave velocity, both at surface and in depth.

A4.3. Free Shape Anomalies Test

[67] To corroborate that the anomalies of the final model could be recovered, this test was performed. We introduced an input model with horizontal anomalies similar to the final model obtained after the inversion of experimental data. This allowed us to check the stability of the geometry and size of the resulting anomalies. The input model at a depth of −3.0 km is seen in Figure A6a, while Figures A6b–A6f plot the recovered anomalies at respective depths of 0.0 km, −3.0 km, −5.0 km, −6.0 km and −7.3 km. The fine horizontal resolution achieved provides imagery of anomalies of different sizes and shapes at depths as great as −7.3 km. Note that the large magnitudes of anomalies are robustly resolved in this test which proves that the amplitudes reported for the main model based on experimental data are close to the reality.

[68] The results of the different resolution tests show that our final seismic velocity model is well resolved at as much as 8 km in depth, and it is a sound indicator of the inner physical properties of this volcanic environment.

[69] Note that all synthetic tests demonstrate fairly good resolution in central part of the Island where most stations are located. However, in the peripheral offshore parts, strong smearing is observed, so the results should be interpreted with prudence.

[70] **Acknowledgments.** We thank all participants in the TOM-TEIVEVS experiment, including the Spanish Army and Navy, the Marine Technology Unit, and the components of the TOM-TEIDEVS Working Group. We also thank Carmen Romero for her valuable comments and suggestions. This work has been partially funded by projects CGL2004-05744-C04-01 and CGL2005-07589-C03-02/ANT of the Spanish Ministry of Science, FP6-2004-Global-3-018471 of the European Union, and by the Geophysics Research Group (RNM104) of the Junta de Andalucía, Spain. The seismic instruments and data management facilities were provided under loan 812 by SEIS-UK at the University of Leicester to the University of Liverpool. Data collected will be available through the IRIS Data Management Center. The facilities of SEIS-UK are supported by the Natural Environment Research Council under Agreement R8/H10/64.

References

Ablay, G. J., G. G. J. Ernst, J. Martí, and R. S. J. Sparks (1995), The 2 ka subplinian eruption of Montaña Blanca, Tenerife, *Bull. Volcanol.*, *57*, 337–355, doi:10.1007/BF00301292.

Almendros, J., J. M. Ibáñez, G. Alguacil, J. Morales, E. Del Pezzo, M. La Rocca, R. Ortiz, V. Araña, and M. J. Blanco (2000), A double seismic antenna experiment at Teide volcano: Existence of local seismicity and lack of evidences of volcanic tremor, *J. Volcanol. Geotherm. Res.*, *103*, 439–462, doi:10.1016/S0377-0273(00)00236-5.

Almendros, J., J. M. Ibáñez, E. Carmona, and D. Zandomeneghi (2007), Array analyses of volcanic earthquakes and tremor recorded at Las Cañadas caldera (Tenerife Island, Spain) during the 2004 seismic activation of Teide volcano, *J. Volcanol. Geotherm. Res.*, *160*, 285–299.

Aloisi, M., O. Cocina, G. Neri, B. Orecchio, and E. Privitera (2002), Seismic tomography of the crust underneath the Etna volcano, Sicily, *Phys. Earth Planet. Inter.*, *134*, 139–155, doi:10.1016/S0031-9201(02)00153-X.

Ancochea, E., J. M. Cantagrel, J. M. Fuster, M. J. Huertas, and N. O. Arnaud (1998), Comment to "Vertical and lateral collapses on Tenerife (Canary Islands) and other volcanic ocean islands" by J. Martí, M. Hurlimann, G. J. Ablay and A. Gudmundsson, *Geology*, *26*, 861–863, doi:10.1130/0091-7613(1998)026<0861:VALCOT>2.3.CO;2.

Ancochea, E., J. Fuster, E. Ibarrola, A. Cendrero, J. Coello, F. Hernán, J. Cantagrel, and C. Jamond (1990), Volcanic evolution of the island of Tenerife (Canary Islands) in the light of the new K-Ar data, *J. Volcanol. Geotherm. Res.*, *44*, 231–249, doi:10.1016/0377-0273(90)90019-C.

Ancochea, E., J. L. Brändle, and M. J. Huertas (1995), Alineaciones de centros volcánicos en la isla de Tenerife, *Geogaceta*, *17*, 56–59.

Ancochea, E., M. J. Huertas, J. M. Cantagrel, J. Coello, J. M. Fúster, N. Arnaud, and E. Ibarrola (1999), Evolution of the Cañadas Edifice and its implications for the origin of the Cañadas Caldera (Tenerife, Canary Islands), *J. Volcanol. Geotherm. Res.*, *88*, 177–199, doi:10.1016/S0377-0273(98)00106-1.

Andújar, J., F. Costa, J. Martí, J. A. Wolff, and M. R. Carroll (2008), Experimental constraints on pre-eruptive conditions of phonolitic magma from the caldera-forming El Abrigo eruption, Tenerife (Canary Islands), *Chem. Geol.*, *257*, 173–191, doi:10.1016/j.chemgeo.2008.08.012.

Anguita, F., and F. Hernán (2000), The Canary Islands origin: A unifying model, *J. Volcanol. Geothem. Res.*, *103*, 1–26.

Aoki, Y., et al. (2009), P wave velocity structure beneath Asama volcano, Japan, inferred from active source seismic experiment, *J. Volcanol. Geotherm. Res.*, *187*, 272–277, doi:10.1016/j.jvolgeores.2009.09.004.

Araña, V., J. Martí, A. Aparicio, L. García Cacho, and R. García (1994), Magma mixing in alkaline magmas: An example from Tenerife, Canary Islands, *Lithos*, *32*, 1–19, doi:10.1016/0024-4937(94)90018-3.

Araña, V., A. G. Camacho, A. García, F. G. Montesinos, I. Blanco, R. Vieira, and A. Felpeto (2000), Internal structure of Tenerife (Canary Islands) based on gravity, aeromagnetic and volcanological data, *J. Volcanol. Geotherm. Res.*, *103*, 43–64, doi:10.1016/S0377-0273(00)00215-8.

Benz, H. M., B. A. Chouet, P. B. Dawson, J. C. Lahr, R. A. Page, and J. A. Hole (1996), Three-dimensional P and S wave velocity structure of Redoubt Volcano, Alaska, *J. Geophys. Res.*, *101*, 8111–8128, doi:10.1029/95JB03046.

Blanco-Montenegro, I., I. Nicolosi, A. Pignatelli, A. García, and M. Chiappini (2011), New evidence about the structure and growth of ocean island volcanoes from aeromagnetic data: The case of Tenerife, Canary Islands, *J. Geophys. Res.*, *116*, B03102, doi:10.1029/2010JB007646.

Calvert, A., S. L. Klemperer, N. Takahashi, and B. C. Kerr (2008), Three-dimensional crustal structure of the Mariana island arc from seismic tomography, *J. Geophys. Res.*, *113*, B01406, doi:10.1029/2007JB004939.

Canales, J. P., J. J. Dañobeitia, and A. B. Watts (2000), Wide-angle seismic constraints on the internal structure of Tenerife, Canary Islands, *J. Volcanol. Geotherm. Res.*, *103*, 65–81, doi:10.1016/S0377-0273(00)00216-X.

Canas, J., A. Ugalde, L. Pujades, J. Carracedo, V. Soler, and M. Blanco (1998), Intrinsic and scattering seismic wave attenuation in the Canary Islands, *J. Geophys. Res.*, *103*(B7), 15,037–15,050, doi:10.1029/98JB00769.

Cantagrel, J. M., N. O. Arnaud, E. Ancochea, J. M. Fuster, M. J. Huertas (1999), Repeated debris avalanches on Tenerife and genesis of Las Cañadas caldera wall (Canary Islands), *Geology*, *27*, 739–742.

Cardaci, C., M. Coviello, G. Lombardo, G. Patané, and R. Scarpa (1993), Seismic tomography of Etna volcano (1993), *J. Volcanol. Geotherm. Res.*, *56*, 357–368, doi:10.1016/0377-0273(93)90002-9.

Carracedo, J. C. (1994), The Canary Islands: An example of structural control on the growth of large oceanic-island volcanoes, *J. Volcanol. Geotherm. Res.*, *60*, 225–241, doi:10.1016/0377-0273(94)90053-1.

Carracedo, J. C., H. Guillou, E. Rodríguez Badiola, F. J. Pérez-Torrado, A. Rodríguez González, R. Paris, V. Troll, S. Wiesmaier, A. Delcamp, and J. L. Fernández-Turiel (2009), La dorsal NE de Tenerife: Hacia un modelo del origen y evolución de los rifts de islas oceánicas, *Estud. Geol.*, *65*(1), 5–47, doi:10.3989/egeol.39755.056.

Coppo, N., P. A. Schnegg, W. Heise, P. Falco, and R. Costa (2008), Multiple caldera collapses inferred from the shallow electrical resistivity signature of the Las Cañadas caldera, Tenerife, Canary Islands, *J. Volcanol. Geotherm. Res.*, *170*, 153–166, doi:10.1016/j.jvolgeores.2007.09.013.

Dawson, P. B., B. A. Chouet, P. G. Okubo, A. Villaseñor, and H. M. Benz (1999), Three-dimensional velocity structure of the Kilauea caldera, Hawaii, *Geophys. Res. Lett.*, *26*, 2805–2808, doi:10.1029/1999GL005379.

DelPezzo, E., M. La Rocca, and J. M. Ibáñez (1997), Observations of high-frequency scattered waves using dense arrays at Teide volcano, *Bull. Seismol. Soc. Am.*, *87*, 1637–1647.

Di Stefano, R., and C. Chiarabba (2002), Active source tomography at Mt. Vesuvius: Constraints for the magmatic system, *J. Geophys. Res.*, *107*(B11), 2278, doi:10.1029/2001JB000792.

Dóniz, J., C. Romero, E. Coello, C. Guillén, N. Sánchez, L. García-Cacho, and A. García (2008), Morphological and statistical characterization of recent mafic volcanism on Tenerife (Canary Islands, Spain), *J. Volcanol. Geotherm. Res.*, *173*, 185–195, doi:10.1016/j.jvolgeores.2007.12.046.

Dóniz Páez, J. (2009), Volcanes basálticos monogénicos de Tenerife, *Rev. Electr. Geogr. Cienc. Soc.*, *14*, 324.

Evangelidis, C. P., T. A. Minshull, and T. J. Henstock (2004), Three-dimensional crustal structure of Ascension Island from active source seismic tomography, *Geophys. J. Int.*, *159*, 311–325.

Flecha, I., D. Martí, R. Carbonell, J. Escuder-Viruete, and A. Pérez Estaún (2004), Imaging low velocity anomalies with the aid of seismic tomography, *Tectonophysics*, *388*, 225–238, doi:10.1016/j.tecto.2004.04.031.

García, A., R. Ortiz, J. M. Marrero, N. Sánchez, M. Tárraga, J. Vila, A. M. Correig, R. Macià, and R. Sleeman (2006), Monitoring the reawakening of Canary Islands' Teide volcano, *Eos Trans. AGU*, *87*(6), 61–65, doi:10.1029/2006EO060001.

García-Yeguas, M. A. (2010), Estudio de heterogeneidades laterales de volcanes activos: Tomografía sísmica de alta resolución de la Isla de Tenerife, anomalías de propagación de ondas sísmicas de la Isla Decepción y otros efectos, PhD thesis, Univ. de Granada, Granada, Spain.

Geyer, A., and J. Martí (2010), The distribution of basaltic volcanism on Tenerife, Canary Islands: Implications on the origin and dynamics of the rift systems, *Tectonophysics*, *483*, 310–326, doi:10.1016/j.tecto.2009.11.002.

Gottsmann, J., A. G. Camacho, J. Martí, L. Wooller, J. Fernández, A. García, and H. Rymer (2008), Shallow structure beneath the central volcanic complex of Tenerife from new gravity data: Implications for its evolution and recent reactivation, *Phys. Earth Planet. Inter.*, *168*, 212–230, doi:10.1016/j.pepi.2008.06.020.

Guillou, H., J. C. Carracedo, R. Paris, and F. Pérez-Torrado (2004), Implications for the early shield-stage evolution of Tenerife from K/Ar ages and magnetic stratigraphy, *Earth Planet. Sci. Lett.*, *222*, 599–614, doi:10.1016/j.epsl.2004.03.012.

Hernández, P., N. Pérez, J. Salazar, M. Sato, K. Notsu, and H. Wakita (2000), Soil gas CO2, CH4 and H2 distribution in and around las Cañadas caldera, Tenerife, Canary Islands, Spain, *J. Volcanol. Geotherm. Res.*, *103*, 425–438, doi:10.1016/S0377-0273(00)00235-3.

Hernández, P. A., N. M. Pérez, J. Salazar, R. Ferrell, and C. Álvarez (2004), Soil volatile mercury, boron and ammonium distribution at las Cañadas caldera, Tenerife, Canary Islands, Spain, *Appl. Geochem.*, *19*(6), 819–834, doi:10.1016/j.apgeochem.2003.12.003.

Huertas, M. J., N. O. Arnaud, E. Ancochea, J. M. Cantagrel, and J. M. Fúster (2002), 40Ar/39Ar stratigraphy of pyroclastic units from the Cañadas Volcanic Edifice (Tenerife, Canary Islands) and their bearing on the structural evolution, *J. Volcanol. Geotherm. Res.*, *115*, 351–365, doi:10.1016/S0377–0273(01)00331–6.

Hürlimann, M., J. Martí, and A. Ledesma (2004), Morphological and geological aspects related to large slope failures on oceanic islands: The huge La Orotava landslides on Tenerife, Canary Islands, *Geomorphology*, *62*, 143–158, doi:10.1016/j.geomorph.2004.02.008.

Ibáñez, J. M., A. Rietbrock, and A. García-Yeguas (2008), Imaging an active volcano edifice at Tenerife Island, Tenerife Island, Spain, *Eos Trans. AGU*, *89*(32), 289–290, doi:10.1029/2008EO320001.

Koulakov, I. (2009), Lotos code for local earthquake tomographic inversion: Benchmarks for testing tomographic algorithms, *Bull. Seismol. Soc. Am.*, *99*, 194–214, doi:10.1785/0120080013.

Koulakov, I., E. I. Gordeev, N. L. Dobretsov, V. A. Vernikovsky, S. Senyukov, and A. Jakovlev (2011), Feeding volcanoes of the Kluchevskoy group from the results of local earthquake tomography, *Geophys. Res. Lett.*, *38*, L09305, doi:10.1029/2011GL046957.

Leonhardt, R., and H. C. Soffel (2006), The growth, collapse and quiescence of Teno volcano, Tenerife: New constraints from paleomagnetic data, *Int. J. Earth Sci.*, *95*, 1053–1064, doi:10.1007/s00531-006-0089-3.

Martí, J., and A. Gudmundsson (2000), The las Cañadas caldera (Tenerife, Canary Islands): An overlapping collapse caldera generated by magma-chamber migration, *J. Volcanol. Geotherm. Res.*, *103*, 161–173, doi:10.1016/S0377-0273(00)00221-3.

Martí, J., J. Mitjavila, and V. Araña (1994), Stratigraphy, structure and geochronology of the Las Cañadas Caldera (Tenerife, Canary Islands), *Geol. Mag.*, *131*, 715–727.

Martí, J., G. J. Ablay, and S. Bryan (1996), Comment on "The Canary Islands: an example of structural control on the growth of large oceanic-island volcanoes" by J.C. Carracedo, *J. Volcanol. Geotherm. Res.*, *72*, 143–149, doi:10.1016/0377-0273(95)00079-8.

Martí, J., M. Hürlimann, G. J. Ablay, and A. Gudmundsson (1997), Vertical and lateral collapses on Tenerife (Canary Islands) and other volcanic ocean islands, *Geology*, *25*(10), 879–882, doi:10.1130/0091-7613(1997)025<0879:VALCOT>2.3.CO;2.

Martí, J., C. Soriano, I. Galindo, and R. A. F. Cas (2010), Resolving problems with the origin of las Cañadas caldera (Tenerife, Canary Islands): Los Roques de García formation-part of a major debris avalanche or an in situ, stratified, edifice-building succession?, *Spec. Pap. Geol. Soc. Am.*, *464*, 113–132, doi:10.1130/2010.2464(06).

Masson, D. G., A. B. Watts, M. J. R. Gee, R. Urgeles, N. C. Mitchell, T. P. Le Bas, and M. Canals (2002), Slope failures on the flanks of the western Canary Islands, *Earth Sci. Rev.*, *57*, 1–35, doi:10.1016/S0012-8252(01)00069-1.

Navarro, J. M., and J. Coello (1989), Depressions originated by landslide processes in Tenerife, paper presented at Meeting on Canarian Volcanism, Eur. Sci. Found., Lanzarote, Spain.

Paige, C. C., and M. A. Saunders (1982), LSQR: An algorithm for sparse linear equations and sparse least squares, *Trans. Math. Software*, *8*, 43–71, doi:10.1145/355984.355989.

Paulatto, M., et al. (2010), Upper crustal structure of an active volcano from refraction/reflection tomography, Montserrat, Lesser Antilles, *Geophys. J. Int.*, *180*, 685–696, doi:10.1111/j.1365-246X.2009.04445.x.

Paulatto, M., C. Annen, T. J. Henstock, E. Kiddle, T. A. Minshull, R. S. J. Sparks, and B. Voight (2012), Magma chamber properties from integrated seismic tomography and thermal modeling at Montserrat, *Geochem. Geophys. Geosyst.*, *13*, Q01014, doi:10.1029/2011GC003892.

Pérez, N. M., S. Nakai, H. Wakita, P. A. Hernández, and J. M. Salazar (1996), Helium-3 emission in and around Teide volcano, Tenerife, Canary Islands, Spain, *Geophys. Res. Lett.*, *23*, 3531–3534, doi:10.1029/96GL03470.

Pous, J., W. Heise, P. A. Schnegg, G. Muñoz, J. Martí, and C. Soriano (2002), Magnetotelluric study of the las Cañadas caldera Tenerife, Canary Islands: Structural and hydrogeological implications, *Earth Planet. Sci. Lett.*, *204*, 249–263, doi:10.1016/S0012-821X(02)00956-1.

Romero, C. (1991), *Las manifestaciones volcánicas históricas del archipiélago canario*, 1463 pp., Cons. de Polít. Territ., Gobierno Autónomo de Canarias, Santa Cruz de Tenerife, Spain.

Romero, C. (1992), *Estudio geomorfológico de los volcanes históricos de Tenerife*, 265 pp., Cabildo Insular de Tenerife, Santa Cruz de Tenerife, Spain.

Sallarès, V., P. Charvis, E. R. Flueh, and J. Bialas (2003), Seismic structure of Cocos and Malpelo Volcanic Ridges and implications for hot spot-ridge interaction, *J. Geophys. Res.*, *108*(B12), 2564, doi:10.1029/2003JB002431.

Schmincke, H. U. (2004), *Volcanism*, 324 pp., Springer, Berlin, doi:10.1007/978-3-642-18952-4.

Shalev, E., et al. (2010), Three-dimensional seismic velocity tomography of Montserrat from the SEA-CALIPSO offshore/onshore experiment, *Geophys. Res. Lett.*, *37*, L00E17, doi:10.1029/2010GL042498.

Thirlwall, M. F., B. S. Singer, and G. F. Marriner (2000), 39Ar-40Ar ages and geochemistry of the basaltic shield stage of Tenerife, Canary Islands, Spain, *J. Volcanol. Geotherm. Res.*, *103*, 247–297, doi:10.1016/S0377-0273(00)00227-4.

van der Sluis, A., and H. A. van der Vorst (1987), *Numerical Solution of Large, Sparse Linear Algebraic Systems Arising From Tomographic Problems. Seismic Tomography*, edited by G. Nolet, Reidel, Dortrecht, Netherlands.

Zandomeneghi, D., J. Almendros, J. M. Ibáñez, and G. Saccorotti (2008), Seismic tomography of central Sao Miguel, Azores, *Phys. Earth Planet. Inter.*, *167*, 8–18, doi:10.1016/j.pepi.2008.02.005.

Zandomeneghi, D., A. H. Barclay, J. Almendros, J. M. Ibáñez, W. S. D. Wilcock, and T. Ben-Zvi (2009), Crustal structure of Deception Island volcano from P wave seismic tomography: Tectonic and volcanic implications, *J. Geophys. Res.*, *114*, B06310, doi:10.1029/2008JB006119.

Zelt, C. A., and P. J. Barton (1998), Three-dimensional seismic refraction tomography: A comparison of two methods applied to data from the Faroe Basin, *J. Geophys. Res.*, *103*, 7187–7210.

Zollo, A., L. D'Auria, R. De Matters, A. Herrero, J. Virieux, and P. Gasparini (2002), Bayesian estimation of 2d p-velocity models from active seismic arrival time data: Imaging of the shallow structure of Mt. Vesuvius (southern Italy), *Geophys. J. Int.*, *151*, 566–582, doi:10.1046/j.1365-246X.2002.01795.x.

Zollo, A., et al. (2003), Evidence for the buried rim of Campi Flegrei caldera from 3D active seismic imaging, *Geophys. Res. Lett.*, *30*(19), 2002, doi:10.1029/2003GL018173.